CrystEngComm

Accepted Manuscript

This is an *Accepted Manuscript*, which has been through the Royal Society of Chemistry peer review process and has been accepted for publication.

Accepted Manuscripts are published online shortly after acceptance, before technical editing, formatting and proof reading. Using this free service, authors can make their results available to the community, in citable form, before we publish the edited article. We will replace this *Accepted Manuscript* with the edited and formatted *Advance Article* as soon as it is available.

You can find more information about *Accepted Manuscripts* in the Information for Authors.

Please note that technical editing may introduce minor changes to the text and/or graphics, which may alter content. The journal's standard Terms & Conditions and the Ethical guidelines still apply. In no event shall the Royal Society of Chemistry be held responsible for any errors or omissions in this *Accepted Manuscript* or any consequences arising from the use of any information it contains.

ROYAL SOCIETY OF CHEMISTRY

www.rsc.org/crystengcomm

A series of d^{10} metal coordination polymers based on a flexible bis(2-methylbenzimidazole) ligand and different carboxylates: synthesis, structures, photoluminescence and catalytic properties

Jin-ming Hao[a], Bao-yi Yu[b], Kristof Van Hecke[b], Guang-hua Cui[a,]*

a College of Chemical Engineering, Hebei United University, 46 West Xinhua Road, Tangshan, 063009, Hebei, PR China

b Department of Inorganic and Physical Chemistry, Ghent University, Krijgslaan 281 S3, 9000 Ghent, Belgium

*Corresponding author. Fax: +86-0315-2592170. Tel: +86-0315-2592169.

*Corresponding author. E-mail: tscghua@126.com.

***To CrystEngComm* (Article)**

CrystEngComm Accepted Manuscript

Abstract

To explore the influence of different aromatic polycarboxylates on the self-assembly and properties of d^{10} metal coordination frameworks, six coordination compounds containing a flexible bis(2-methylbenzimidazole) (pbmb) ligand, formulated as, $[Ag_2(pbmb)(2,6\text{-napdc})]_n$ (**1**), $\{[Zn(pbmb)(tbta)]\cdot H_2O\}_n$ (**2**), $\{[Cd(pbmb)(tbta)]\cdot H_2O\}_n$ (**3**), $[Zn_2(pbmb)(btec)(H_2O)]_n$ (**4**), $\{[Zn_2(OH)(pbmb)(bpdc)_{1.5}]\cdot H_2O\}_n$ **(5)**, $[Cd(pbmb)(3\text{-npa})(H_2O)]_n$ (**6**) have been synthesized under hydrothermal conditions and characterized by physicochemical and spectroscopic methods as well as single-crystal X-ray diffraction analysis. (2,6-H_2napdc = 2,6-naphthalenedicarboxylic acid, H_2tbta = tetrabromoterephthalic acid, H_4btec = 1,2,4,5-benzenetetracarboxylic acid, H_2bpdc = biphenyl-4,4'-dicarboxylic acid and $H_2$3-npa = 3-nitrophthalic acid). Complexes **1** possesses a 8-connected 3D coordination framework with **sqc3** topoly based on rare tetranuclear Ag(I)-cluster secondary building units (SBUs). **2** and **3** posses 2D (4,4) grid structures. **4** shows a novel (3,4,5)-connected 2D network with the Schläfli symbol of $\{3.4.5\}\{3.4^2.5^2.6\}\{3.4^3.5^3.6.7^2\}$. **5** features an uninodal (4,4)-connected net containing binuclear $\{Zn_2(OH)\}$ SBUs and a 2-fold interpenetrating (3,6)-connected supramolecular framework with $\{4^2.6\}\{4^4.6^{10}.8\}$-**3,6T24** topology is formed *via* hydrogen bond interactions. Complex **6** is a 1D double-chain structure, which is finally extended to a 3D (4,5,5)-connected supramolecular network *via* hydrogen bonding interactions. Complexes **1**-**6** indicate high thermalt s abilities and different photoluminescence behavior in the solid state. Moreover, all of these polymer materials manifest excellent photocatalytic activities for the degradation of methyl orange in the photo-Fenton-like process after 120 min. (**1**: 99%, **2**: 66%, **3**: 91%, **4**: 83%, **5**: 91% and **6**: 93%, respectively).

CrystEngComm Accepted Manuscript

Introduction

The design and assembly of metal–organic frameworks (MOFs) has become an important research branch in coordination chemistry and crystal engineering, not only for the potential applications of MOFs as functional materials in catalysis, fluorescence, gas adsorption/separation and magnetism, but also for their diverse structures and novel topologies [1–4]. Noteworthy, the construction of intriguing and useful MOFs, influenced by different factors (metal ions, organic ligands, solvent system, pH value and reaction temperature, etc.)[5], is of tremendous challenge in the fields of coordination chemistry and crystal engineering. In the last two decades, much effort has been focused on the rational design and controlled synthesis of MOFs using multidentate ligands, such as polycarboxylate and N-heterocyclic ligands. Usually, organic ligands with bent backbones, e.g. V-shaped, triangular, quadrangular, and so on, are excellent candidates for building high-connected, interpenetrating, or helical coordination frameworks due to their bent backbones and versatile bridging fashions [6, 7]. Relative to rigid N-donor ligands, flexible N-donor ligands have more advantages, because their flexibility and conformational freedom allow them to conform to the coordination environment of metal ions [8]. In the previous work from our and other groups, based on a series of bis(2-methylbenzimidazole) ligands with $–(CH_2)_n–$ backbones, many marvelous architectures were successfully obtained [9]. Meanwhile, we found that the $–(CH_2)_n–$ backbone and the 2-position substituent methyl group could strengthen the coordination ability of the ligands with metal ions [10,11]. On the one hand, by using the bis(2-methylbenzimidazole) ligand as a versatile scaffold, a systematic research of the multidimensional MOFs regarding the impact of different auxiliary aromatic polycarboxylates would be feasible and valuable. The aromatic polycarboxylic acid organic building blocks(such as 2,6-H_2napdc = 2,6-naphthalenedicarboxylic acid, H_2tbta = tetrabromoterephthalic acid, H_4btec = 1,2,4,5-benzenetetracarboxylic acid, H_2bpdc = biphenyl-4,4'-dicarboxylic acid and $H_2$3-npa = 3-nitrophthalic acid), with triangular and linear geometries, have been proved as versatile linkers to connect metal ions into higher dimensional structures through various coordination modes, as well as secondary interactions such as hydrogen

CrystEngComm Accepted Manuscript

bond and halogen bond.

Textile industries produce a great deal of wastewater, which is polluted by the presence of dyes. Azo dyes constitute the largest and the most important class of commercially available dyes, accounting for 50% of all commercial dyes [12]. The release of these compounds into water streams is undesirable, not only because of their color, but also because many azo dyes are known to cause ecological and environmental problems because they are toxic, non-biodegradable and potentially carcinogenic [13]. At present, these dyes can be abated by some non-destructive processes, such as coagulation, activated carbon adsorption and membrane filtration. Advance oxidation processes (AOPs) are increasingly used as for the reduction of organic contaminants in a variety of wastewaters from different industrial plants [14, 15]. Persulfate ($S_2O_8^{2-}$) is one of the strongest oxidants known in aqueous solutions and has an even higher potential ($E^{\ominus}$ = 2.01 V) than H_2O_2 (E^{ψ} = 1.76 V). Compared with other oxidants, it has advantages due to its facile storage and transport, high stability, high aqueous solubility and relatively low cost [16]. To date, some researchers have proved that the transition metal coordination complexes exhibit prominent catalytic activities in Fenton-like process. The different catalytic performances of these metal complexes may be due to the distinct coordination environments around the metal centers or molecular structures [9]. The present research work highlights the utility of sodium persulfate instead of H_2O_2 as an oxidant in the classical photo-Fenton process, which is termed as photo-Fenton-like process for the degradation of methyl orange azo dye [9]. In addition, some d^{10} MOFs constructed from aromatic polycarboxylates display photocatalytic activity for degrading certain organic contaminants have been reported previously[9k]. As an electron (e^-) and hole (h^+) transfer process driven by light, the photocatalysis is controlled by several influences. The optical band gap (Eg) and the sorption of O_2/OH^- on the MOFs are two of the key factors, which are distinctly connected with the constructions of the MOFs[9].

To investigate the influence of different organic carboxylates anions on the crystal structures and properties of the resulting d^{10} metal coordination polymers containing

CrystEngComm Accepted Manuscript

1,1'-(1,3-propane)bis-(2-methylbenzimidazole) (pbmb) ligand. Six compounds, namely $[Ag_2(pbmb)(2,6\text{-napdc})]_n$ (**1**), $\{[Zn(pbmb)(tbta)]\cdot H_2O\}_n$ (**2**), $\{[Cd(pbmb)(tbta)]\cdot H_2O\}_n$ (**3**), $[Zn_2(pbmb)(btec)(H_2O)]_n$ (**4**), $\{[Zn_2(OH)(pbmb)(bpdc)_{1.5}]\cdot H_2O\}_n$ (**5**) and $[Cd(pbmb)(3\text{-npa})(H_2O)]_n$ (**6**) are reported and the synthetic strategies of **1–6** are presented in Scheme 1. The crystal structure analysis of these complexes, as well as the effect of bis(2-methylbenzimidazole) ligands and different carboxylates on the ultimate frameworks, are also represented and discussed. The thermal stabilities, photoluminescence properties and the optical energy gap of **1-6** have also been investigated. Additionally, photocatalytic activities for the degradation of methyl orange azo dye using the six title compounds as catalysts are surveyed in photo-Fenton-like process.

Experimental section

Materials and physical measurements

The pbmb ligand was synthesized in accordance with the literature (Scheme 2) [17], while the other reagents and solvents employed were commercially available and used as received without any further purification. C, H, and N elemental analyses were carried out with a Perkin-Elmer 240C analyzer. IR spectra were recorded on KBr discs on an Avatar 360 (Nicolet) spectrophotometer in the range of 4000–400 cm^{-1}. Thermogravimetric analysis (TGA) was conducted on a Netzsch TG 209 thermal analyzer under flowing N_2 with a heating rate of 10 °C min^{-1} between ambient temperature and 800 °C. The fluorescence spectra were collected with a Hitachi F-7000 spectrophotometer at room temperature. Powder X-ray diffraction (PXRD) was performed on a Rigaku D/Max-2500 diffractometer at 40 kV, 100 mA with Cu Kα radiation (λ = 1.5418 Å) over the 2θ range of 5–50° at room temperature. The solid-state diffuse-reflectance ultraviolet–visible (UV–Vis) spectra for powder samples were recorded on a UV–Vis spectrophotometer (Puxi, UV 1901) equipped with an integrating sphere with a Praying Mantis diffuse reflectance accessory over the range of 200–800 nm using $BaSO_4$ as the reflectance standard. The concentration of the methyl orange solutions was determined with a UV–Vis

CrystEngComm Accepted Manuscript

spectrophotometer (Puxi, UV 1901).

Synthesis

Synthesis of $[Ag_2(pbmb)(2,6\text{-napdc})]_n$ (1) A mixture of AgOAc (0.1 mmol, 16.7 mg), pbmb (0.1 mmol, 30.4 mg) and 2,6-H_2napdc (0.1 mmol, 21.6 mg) was prepared in H_2O (10 mL) and the pH was adjusted to about 6.5 by the addition of 0.1 mol/dm^3 NaOH. The solution was stirred for 1 h, and then, the resulting mixture was sealed in a Teflon-lined stainless steel vessel (25 mL) and heated to 140 °C for 3 days under autogenous pressure, followed by cooling to room temperature at a rate of 5 °C h^{-1}. Colorless block crystals of **1** were obtained with a yield of 64% based on Ag. Anal. Calcd. for $C_{31}H_{26}Ag_2N_4O_4$ (Mr = 734.30) Calcd: C 50.71, H 3.57 and N 7.63 %. Found: C 51.12, H 3.69 and N 7.88 %. IR (KBr, cm^{-1}): 3418(m), 2947 (m), 1556(s), 1512(m), 1451 (m), 1402(s), 1354(m), 1285(w), 1165(w), 1016(w), 924(w), 859(w), 747(s).

Synthesis of $\{[Zn(pbmb)(tbta)]\cdot H_2O\}_n$ (2) The synthesis procedure of **2** is analogous to that of **1**, except that Ag(OAc) and 2,6-H_2napdc were replaced by $Zn(OAc)_2$ (0.1 mmol, 18.3 mg) and H_2tbta (0.1 mmol, 48.2 mg), respectively. Colorless block crystals of **2** were obtained with a yield of 37% based on Zn. Anal. (%) calcd for $C_{27}H_{22}Br_4N_4O_5Zn$ (Mr = 867.48): C, 37.38; H, 2.56; N, 6.46. Found: C, 37.69; H, 2.74; N, 6.79. IR (KBr, cm^{-1}): 3525(m), 3123(m), 1641(s), 1512(m), 1461(m), 1390(s), 1300(s), 1081(m), 1018(w), 936(w), 820(w), 749(m), 571(m), 530(m), 430(w).

Synthesis of $\{[Cd(pbmb)(tbta)]\cdot H_2O\}_n$ (3) The synthesis procedure of **3** is analogous to that of **2**, except that $Zn(OAc)_2$ was replaced by $Cd(OAc)_2\cdot 2H_2O$ (0.1 mmol, 26.7 mg). Colorless block crystals of **3** were obtained with a yield of 56% based on Cd. Anal. (%) calcd for $C_{27}H_{22}Br_4CdN_4O_5$ (Mr = 914.53): C, 35.46; H, 2.42; N, 6.13. Found: C, 35.66; H, 2.49; N, 6.26. IR (KBr, cm^{-1}): 3430(m), 3025(m), 2943(w), 1610(s), 1511(s), 1479(m), 1458(m), 1402(s), 1320(s), 1078(m), 1009(m), 837(m), 746(s), 576(m), 430(w).

Synthesis of $[Zn_2(pbmb)(btec)(H_2O)]_n$ (4) The synthesis procedure of **4** is analogous to that of **2**, except that H_2tbta was replaced by H_4btec (0.10 mmol, 25.4 mg). Colorless block crystals of **4** were obtained with a yield of 61% based on Zn. Anal. (%) calcd for $C_{29}H_{24}N_4O_9Zn_2$ (Mr =

CrystEngComm Accepted Manuscript

703.26): C, 49.53; H, 3.44; N, 7.97. Found: C, 51.02; H, 3.61; N, 8.19. IR (KBr, cm^{-1}): 3395(m), 2940(w), 1610(s), 1465(m), 1418(m), 1368(s), 1131(m), 942(m), 759(m), 726(s), 671(w).

Synthesis of $\{[Zn_2(OH)(pbmb)(bpdc)_{1.5}]\cdot H_2O\}_n$ **(5)** The synthesis procedure of **5** is analogous to that of **2**, except that H_2tbta was replaced by H_2bpdc (0.10 mmol, 24.2 mg). Colorless block crystals of **5** were obtained with a yield of 73% based on Zn. Anal. (%) calcd for $C_{40}H_{35}N_4O_8Zn_2$ (Mr = 830.46): C, 57.85; H, 4.25; N, 6.75. Found: C, 58.12; H, 4.13; N, 6.62. IR (KBr, cm^{-1}): 3436(m), 2974(m), 1677(s), 1602(s), 1545(s), 1514(m), 1458(m), 1390(s), 1296(s), 1174(m), 932(m), 840(m), 762(s), 680(w), 551(w).

Synthesis of $[Cd(pbmb)(3\text{-npa})(H_2O)]_n$ **(6)** The synthesis procedure of **6** is analogous to that of **2**, except that $Zn(OAc)_2$ and H_2tbta were replaced by $Cd(OAc)_2\cdot 2H_2O$ (0.1 mmol, 26.7 mg) and $H_2$3-npa (0.10 mmol, 21.1 mg), respectively. Colorless block crystals of **6** were obtained with a yield of 55% based on Cd. Anal. (%) calcd for $C_{27}H_{25}CdN_5O_7$ (Mr = 643.92): C, 50.36; H, 3.91; N, 10.88. Found: C, 50.63; H, 4.12; N, 11.01. IR (KBr, cm^{-1}): 3416(m), 2927 (m), 1555(s), 1512(s), 1481 (m), 1460(m), 1413(s), 1292(w), 1151(w), 859(w), 744(s), 685(w).

Crystal data collection and refinement

The data for complexes **1–6** were collected on a Bruker Smart 1000 CCD diffractometer using graphite-monochromated Mo *Kα* radiation (λ = 0.71073 Å) with ω-scan mode at 293 K. A semi-empirical absorption correction was applied using the SADABS program[18]. The structures were solved by direct methods and refined on F^2 by full-matrix least-squares using SHELX-2014[19]. All non-hydrogen atoms were refined anisotropically. Hydrogen atoms of coordinated and uncoordinated water molecules were located in a difference Fourier map, while other hydrogen atoms were included in calculated positions and refined with isotropic thermal parameters riding on the parent atoms. One lattice water molecule for complex **5** is disordered, and this structure was refined by the SQUEEZE routine of PLATON[20]. Crystallographic crystal data and structure processing parameters for **1–6** are summarized in Table S1 (Support Information). Selected bond lengths and bond angles of **1–6** are listed in Table S2.

CrystEngComm Accepted Manuscript

Crystallographic data for **1–6** have been deposited at the Cambridge Crystallographic Data Centre with CCDC reference numbers 1026130 for **1**, 1027222 for **2**, 1026132 for **3**, 1026133 for **4**, 1026134 for **5** and 1026131 for **6**.

Catalytic experimental procedures

The catalytic performance of the complexes were investigated for the degradation of methyl orange through a typical process as follows: 0.01 mmol solid catalysts (**1-6**) and 0.04 mmol sodium persulfate (the molar ratio catalyst/persulfate is about 1:4) were mixed together with 100 mL of methyl orange solution (10 mg/L) and the pH was adjusted to different pH values by dropwise addition of 0.1 mol/L H_2SO_4 or 0.1 mol/L NaOH. The mixture was magnetically stirred for half an hour in a dark environment to get a uniform working solution. The photocatalytic degradation of methyl orange was conducted on an XPA-7 type photochemical reactor (Xujiang Machine Factory, Nanjing, China) [21] equipped with a 100 W mercury lamp (mean wavelength 365 nm) with light intensities at quartz tube positions of 12.7 mW/cm^2 (measured using a UV-A irradiation meter, Beijing Normal University, China). The temperatures of the reaction solutions were maintained at 25±1 ºC by cooling water circulation. 3 mL of the suspension was taken at given time intervals and separated through centrifugation and then subsequently analyzed by UV-visible spectrometer at a special wavelength. When the pH value of the methyl orange is above 3.0, the absorbance maximum is 464 nm, while the pH value is 3.0 the absorbance maximum is 469 nm, and the pH value is less than 3.0, the absorbance maximum is 506 nm. In addition, the control experiment for methyl orange degradation was also performed at the same condition without catalyst.

The degradation efficiency of methyl orange is defined by the initial absorbance values of the dye solution (A_0) and the absorbance values of the dye solution at reaction time (A_t):

$$\text{Degradation efficiency} = \frac{A_0 - A_t}{A_0} \times 100\% \qquad (1)$$

The stability of the compounds after photocatalytic process has been experiment through

CrystEngComm Accepted Manuscript

PXRD. Total organic carbon (TOC) measured with a Sievers 900 TOC analyser by injection of appropriate volume of sample at different time intervals during irradiation. The results are expressed as TOC/TOC_0 where TOC is total organic carbon at time t, and TOC_0 = initial total organic carbon of methyl orange (10 mg L^{-1}). The mineralization degrees were determined only at the end of each experiment.

Results and discussion

Synthesis and structures

The assembly of a coordination polymer is heavily influenced by the ligand conformation and the coordination geometry of the metal ions. The hydrothermal synthesis method can cause a reaction to shift from the kinetic to the thermodynamic domain and it has been extensively explored as an effective and powerful tool in the self-assembly of MOFs, especially for high-dimensional frameworks. MOFs **1–6** were generated by hydrothermal reaction of carboxylates and bis(methylbenzimidazole) with different transition metal salts (Cd(II), Zn(II), and Ag(I) salts). On varying the molar ratio and composition of the initial reactants, reaction time, and temperature, single crystals of complexes **1-6** suitable for X-ray single-crystal diffraction analysis are successfully obtained. The results of elemental analysis for the complexes were in good agreement with the theoretical requirements of their compositions calculated from the X-ray structural analysis. Compounds **1-6** are stable at room temperature and not soluble in water and common organic solvents such as, alcohol, and acetonitrile as well as chloroform and toluene.

Crystal structure of $[Ag_2(pbmb)(2,6\text{-napdc})]_n$ (1)

Single crystal X-ray diffraction analysis indicated that **1** crystallizes in the monoclinic crystal system and $P2_1/n$ space group. The asymmetric unit contains two crystallographically independent Ag(I) ions, one pbmb ligand and one 2,6-napdc^{2-} anion. The Ag1 ion is four-coordinated by one imidazole nitrogen atom from the pbmb ligand (Ag1−N3A =2.221(2) Å) and three carboxyl oxygen atoms (O1C, O2 and O3B) from three distinct 2,6-napdc^{2-} anions (The bond distances of Ag1−O are in the range of 2.309(2)−2.503(2) Å), exhibiting a distorted trigonal pyramidal

CrystEngComm Accepted Manuscript

geometry {AgNO3} with the value of the τ_4 factor being 0.80 [22] (Fig 1a). The Ag2 ion is three-coordinated to two oxygen atoms (O1C and O3D) and one nitrogen atoms (N1) (Ag2−N1=2.175(2) Å and Ag2−O bond lengths are 2.243(2) (Ag2−O3D) and 2.486(2) (Ag2−O1C) Å), showing a triangle {AgNO2} (symmetry code: A: -*x*+1/2,*y*+1/2,-*z*+3/2; B: *x*-1/2,-*y*+5/2,*z*-1/2; C: -*x*,-*y*+2,-*z*+2; D: -*x*+1/2,*y*-1/2,-*z*+5/2).

In **1**, the 2,6-naphthalenedicarboxylic acid is deprotonated completely and acts as a μ_5-bridge linking three Ag1 ions and two Ag2 ions, in which two carboxylate groups adopt two unprecedented μ_3-η^1, η^2 and μ_2-η^2, η^0 coordination fashions, respectively (Fig 1b). It is important to note that four Ag(I) atoms are held together by four carboxyl groups to yield a novel tetranuclear Ag(I)-cluster [$Ag_4(COO)_4$] (Fig. 1c). The distances between the adjacent Ag(I) ions are in the range of 3.256–4.895 Å. Each [$Ag_4(COO)_4$] secondary building (SBU) joins four neighboring 2,6-napdc^{2-} ligands to form a 2D (4,4) layer (Fig. 1d). The pbmb ligands adopt a symmetrical *anti*-conformation with a $N_{donor}\cdots N\text{-}C_{sp3}\cdots C_{sp3}$ torsion angle of 58.078°. The pbmb ligands connect two Ag(I) ions from two different SBUs in a bidentate coordination fashion, which pillars the 2D layer to generate a 3D coordination framework (Fig. 1e). The no-bonding Ag···Ag distance across a pbmb is 11.934 Å. From a topological viewpoint, each tetranuclear SBU is linked to eight [$Ag_4(COO)_4$] SBUs by four 2,6-napdc^{2-} anions and four pbmb ligands, and hence should be considered as an 8-connected node. Because each 2,6-napdc^{2-} anion and pbmb ligand can be viewed as linear linkers, the final 3D framework of **1** can be described as a 8-connected uninodal **sqc3** topology by the TOPOS 4.0 program [23], with a point symbol of {$4^2$4.6^4} (Fig. 1f). To the best of our knowledge, this 3D **sqc3** topology represents the first example of a metal–organic replica based on tetranuclear Ag(I)-cluster SBU.

Crystal structure of {[Zn(pbmb)(tbta)]·H_2O}$_n$ (2)

Single crystal X-ray crystallographic studies reveal that complex **2** crystallizes in the monoclinic crystal system and *P*2/n space group with half of the molecule in the asymmetric unit. The tbta ligand lies about an inversion centre that the Zn1 atom, water O1W and the pbmb ligand

CrystEngComm Accepted Manuscript

lie about a twofold axis. The coordination environment around the Zn^{II} can be described as a distorted $\{ZnO_2N_2\}$ trigonal pyramidal geometry (the value of the τ_4 factor being 0.83) with two oxygen atoms (O2 and O2A) from two different $tbta^{2-}$ anions and two nitrogen atom (N1 and N1A) of two distinct pbmb ligands (symmetry code: A: -*x*+1/2,*y*,-*z*+1/2) (Fig 2a),. The Zn–O2 bond length is 1.978(3) Å and Zn–N distance is 1.993(3) Å. For the $tbta^{2-}$ anion, two carboxyl groups are coordinated to two Zn(II) ions in a monodentate mode. In this manner, the $tbta^{2-}$ anions bridge two adjacent Zn(II) ions generating a $[Zn(tbta)]_n$ straight chain with a Zn···Zn separation of 11.019 Å. In addition, the pbmb, as bridging ligands, link the neighboring two Zn(II) centers forming a $[Zn(pbmb)]_n$ linear chain with the nonbonding Zn···Zn distances of 11.789 Å. The pbmb ligand adopts an asymmetrical *anti*-conformation with a dihedral angle between two benzimidazole rings of 75.248°. The adjacent $[Zn(pbmb)]_n$ chains are bridged by $tbta^{2-}$ ligands forming a (4,4) grid layer (Fig 2b). Furthermore, there exist O–H···O hydrogen bonding interactions between the lattice water molecules and carboxylate oxygen atoms of $tbta^{2-}$ anions, which are further stabilizing this 2D packing (Fig 2c).

In addition, the neighboring 2D layers are finally extended to a 3D supramolecular framework by two kinds of weak $\pi-\pi$ interactions among the benzene rings and imidazole rings of pbmb ligands with a face-to-face distance of 3.468(2) and 3.819(2) Å, respectively (Fig 2d).

Crystal structure of $\{[Cd(pbmb)(tbta)]\cdot H_2O\}_n$ (3)

Single crystal X-ray diffraction analysis indicated that **3** crystallizes in the triclinic crystal system and $P\bar{1}$ space group. The asymmetric unit contains one Cd(II) ion, one pbmb ligand, one lattice water molecule and two half tbta ligands, each lying about inversion centres. The crystallographically independent Cd(II) ion is four-coordinated by two imidazole nitrogen atoms (N1 and N3A) from two distinct pbmb ligands and two oxygen atoms (O1 and O3) from two different $tbta^{2-}$ anions, exhibiting a distorted tetrahedral geometry $\{CdN_2O_2\}$ (Fig 3a). The Cd−O bond distance are 2.201(6) (Cd1−O3) and 2.213(6) Å (Cd1−O1) and the Cd−N bond lengths are 2.182(7) (Cd1-N3A) and 2.185(7) (Cd1-N1) Å (symmetry code: A: *x*,*y*-1,*z*).

CrystEngComm Accepted Manuscript

In **3**, each $tbta^{2-}$ ligand adopts a bis-monodentate coordination mode connecting two adjacent Cd(II) ions to produce a $[Cd(tbta)]_n$ straight chain with a Cd···Cd separation of 11.323 Å. Then two neighboring chains are interlinked by pbmb ligands, with a bridging coordination fashion to give a 2D (4,4) network (Fig 3b). The pbmb ligand connects two Cd(II) ions adopts a asymmetrical *anti*-conformation with the dihedral angle between two benzimidazole rings is 81.302° and the nonbonding Cd···Cd distance of 12.175 Å.

The neighboring 2D layers are finally extended to a 3D supramolecular framework by the $\pi-\pi$ interactions among the benzene rings and imidazole rings of pbmb ligands with center-to-center distance of 3.452 and 3.507 Å, respectively (Fig 3c).

Crystal structure of $[Zn_2(pbmb)(btec)(H_2O)]_n$ (4)

4 is a 2D layer and crystallizes in the triclinic system and $P\bar{1}$ space group, whose asymmetric unit includes two independent Zn(II) ions, a pbmb ligand, a $btec^{4-}$ anion and a coordination water molecule.

The coordination environment around the Zn^{II} atom is shown in Fig 4a. The Zn1 central atom adopts a distorted tetrahedron arrangement by coordinating to two oxygen atoms from two $btec^{4-}$ anions (O6, O8A), one oxygen atom (O1W) from a coordination water molecule and one nitrogen atom (N3B) from one pbmb ligand. The Zn2 atom also adopts a distorted tetrahedral geometry, coordinated by three carboxyl oxygen atoms from three $btec^{4-}$ anions and one nitrogen atom. The Zn−O bond distances vary from 1.9283(16) to 2.0365(16) Å and the Zn−N bond distances are 1.979(2) (Zn1-N3B) and 1.9666(19) (Zn2-N1) Å (symmetry code: A: $-x+2,-y+2,-z-1$; B: $-x+2,-y+2,-z$), which are all within expected ranges [24].

The four carboxyl groups of the $btec^{4-}$ anion are completely deprotonated and adopt the coordination modes of μ_2-η^1:η^1, μ_1-η^0:η^1, μ_1-η^0:η^1 and μ_1-η^0:η^1 (Fig. 4b) to connect Zn(II) atoms to form a 2D layer containing three kinds of rings (Fig. 4c). One is a 14-member ring constructed by two Zn(II) atoms and four carboxyl groups from two $btec^{4-}$ anions. The second ring is a 14-member ring also containing two Zn(II) atoms and four carboxyl groups from two $btec^4$. The

CrystEngComm Accepted Manuscript

third one is a 22-member ring constructed by the connection of six carboxyl groups from four $btec^{4-}$ anions among four Zn(II) atoms. Herein, the pbmb ligand adopts an asymmetrical *syn*-conformation with a $N_{donor}\cdots N\text{-}C_{sp3}\cdots C_{sp3}$ torsion angle of 70.011°, showing a bidentate fashion to join Zn(II) ions in the elliptical ring, which may further stabilize the 2D layers (Fig. 4c).

Furthermore, topological analysis is carried out to get insight in the structure of **4**. The Zn1, Zn2 and $btec^{4-}$ anions act as 3-connected, 4-connected and 5-connected nodes, respectively, giving rise to a (3,4,5)-connected 2D network with the Schläfli symbol of $\{3.4.5\}\{3.4^2.5^2.6\}\{3.4^3.5^3.6.7^2\}$ (Fig. 4d). To the best of our knowledge, among thousands of reported MOFs, the one with this kind of net has never been reported before. Therefore, **4** is an unique metal–organic framework, not only because of the rare coordination modes of $btec^{4-}$ anions but also because of the special (3,4,5)-connected topological structure.

Finally, these 2D sheets are extended into a 3D supramolecular architecture *via* weak $\pi-\pi$ interactions among the benzene rings of $btec^{4-}$ anion or benzimidazole and imidazole rings of pbmb ligands with a face-to-face distance of 3.625(2) and 3.710(2) Å, respectively (Fig 4e).

Crystal structure of $\{[Zn_2(OH)(pbmb)(bpdc)_{1.5}]\cdot H_2O\}_n$ (5)

Complex **5** crystallizes in the monoclinic space group $P2_1/n$. Two Zn(II) ion, one pbmb ligand , one hydroxide anion, one lattice water molecule, one and a half $bpdc^{2-}$ anions in which one of the bpdc ligands lies about an inversion centre consist of the asymmetric unit of **5**. As shown in Fig. 5a, the Zn1 ion adopts a distorted tetrahedron geometry by coordinating to two oxygen atoms from two $bpdc^{2-}$ anions (O1, O4), one oxygen atom (O7) from the μ_2-hydroxide anion and one nitrogen atom from one pbmb ligand (N3). The Zn2 center adopts a trigonal bipyramidal structure defined by three oxygen atoms (O2, O5A and O6A. symmetry code: A: $-x+1,-y+1,-z+2$) from two distinct $bpdc^{2-}$ anions, one oxygen atom (O7) stemming from a μ_2-hydroxide anion and one nitrogen atom from one pbmb ligand (N1B) (symmetry code: B: $x+1,y,z$). Notably, two Zn(II) ions are held together by a μ_2-hydroxide anion to yield a binuclear $\{Zn_2OH\}$ SBU with a Zn···Zn distance of

CrystEngComm Accepted Manuscript

3.143 Å. The bond lengths of Zn–O and Zn–N are similar to those in other zinc coordination complexes.

In **5**, two $bpdc^{2-}$ anions adopt different coordination fashions: two carboxyl groups of one $bpdc^{2}$ coordinated to two Zn(II) ions with the chelating and monodentate mode (μ_1-η^1:η^1 and μ_1-η^0:η^1) and another $bpdc^{2}$ adopts μ_2-η^1:η^1 and μ_2-η^1:η^1 coordination mode connecting four adjacent Zn(II) ions (Fig. 5b). Two kinds of $bpdc^{2-}$ anions bridge the Zn(II) ions alternatively to form a 1D loop-like chain (Fig. 5c). Ligand pbmb adopts an asymmetrical *anti*-conformation with a $N_{donor}\cdots N\text{-}C_{sp3}\cdots C_{sp3}$ torsion angle of 61.890°, which supports the 1D Zn(II)/$bpdc^{2}$ chain to generate a 2D layer (Fig. 5d). The Zn···Zn distance across one pbmb is 11.085 Å. Furthermore, considering the binuclear $\{Zn_2OH\}$ SBU as 4-connected node, and the bridging $bpdc^{2}$ and pbmb ligands are defined as linkers, the 2D framework of **5** can be described as a uninodal (4,4)-connected layer.

In addition, hydrogen bonding interactions exist between hydroxide anions and carboxylate oxygen atoms of $bpdc^{2-}$ anions, extending the 2D layers to a 3D supramolecular architecture. With further topological analysis, the $bpdc^{2-}$ anions can be defined as 3-connected nodes since they bridge three binuclear $\{Zn_2OH\}$ SBUs. The binuclear $\{Zn_2OH\}$ can be simplified as 6-connected nodes. Therefore, the 3D supramolecular structure can be described as a (3,6)-connected 2-fold interpenetrated **3,6T24** topology with a point symbol of $\{4^2.6\}\{4^4.6^{10}.8\}$ (Fig. 5e).

Crystal structure of $[Cd(pbmb)(3\text{-}npa)(H_2O)]_n$ (6)

Compound **6** crystallizes in the triclinic system with P$\bar{1}$ space group. The coordination environment around the Cd(II) atom is shown in Fig. 6a. The central Cd(II) atom adopts a octahedral arrangement by coordinating to four oxygen atoms from two $3\text{-}npa^{2-}$ anions (O1, O2 and O6A) (symmetry code: A: -*x*,-*y*+1,-*z*+2) and one coordinated water molecule (O1W), and two nitrogen atoms from two pbmb ligands (N1 and N4B). The Cd–O bond lengths vary from 2.271(5) to 2.516(5) Å, while Cd–N distances are 2.282(5) and 2.333(5) Å, which are all within standard ranges.

CrystEngComm Accepted Manuscript

In **6**, the carboxylate groups of the 3-npa^{2-} ligands adopt monodentate and chelating coordination modes, pbmb takes on an asymmetric *anti*-conformation with a $N_{donor}\cdots N\text{-}C_{sp3}\cdots C_{sp3}$ torsion angle of 71.530°. Every two pbmb and two 3-npa^{2-} ligands are linked by adjacent Cd(II) ions to form two types of units, $[Cd_2(3\text{-}npa^{2-})_2]$ and $[Cd_2(pbmb)_2]$. The Cd···Cd distances across pbmb and 3-npa^{2-} anions are 9.836 and 5.613 Å, respectively. The two types of units are arranged alternately via metal knots leading to the generation of a 1D double-chain structure (Fig. 6b). The neighboring 1D double-chains are finally extended into a 3D supramolecular framework *via* four types of weak hydrogen bonding interactions between oxygen atoms of carboxylates or coordinated water molecules and carbon atoms (Fig. 6c). To better understand the supermolecular framework of **6**, the topological analysis approach is employed. All Cd(II) centers act as 4-connected nodes, connecting two pbmb ligands and two 3-npa^{2-} anions. And the pbmb ligands implied to be 5-connected nodes bridging two Cd ions and three 3-npa^{2-} anions and then the 3-npa^{2-} are simplified as 5-connected nodes. As a result, the 3D supermolecular network can be reduced as a new trinodal (4,5,5)-connected net with a point symbol of $\{4^2.6^4\}\{4^3.6^7\}\{4^7.6^3\}$ (Fig. 6d).

Influence of the flexible bis(methylbenzimidazole) ligand and carboxylate anions on the architectures of compounds 1−6.

In this study, a flexible ligand pbmb, which has $-(CH_2)_3-$ spacers, was prepared to react with Cd(II), Ag(I) and Zn(II) ions and five carboxylates, yielding six compounds with diverse structures. Our research indicates that bis(methylbenzimidazole) ligands and carboxylates have a significant effect on the architectures of compounds **1−6.**

Compounds **1−6**, based on the same bridging pbmb ligand, have been synthesized by changing the metal salts and carboxylates, which show structural changes from a 3D coordination framework (for **1**), to 2D layers (for **2-5**), and to a 1D double-chain (for **6**). The pbmb ligand exhibits symmetric *anti*-conformation in **1**, asymmetric *anti*-conformation in **2**, **3**, **5**, **and 6** as well as asymmetric *syn*-conformation in **4**. All of the $N_{donor}\cdots N\text{-}C_{sp3}\cdots C_{sp3}$ torsion angles are different.

CrystEngComm Accepted Manuscript

The pbmb ligands adopt the bidentate bridging mode, which connects metal ions thereby leading to various M···M distances: 11.934 Å for **1**, 11.789 Å for **2**, 12.175 Å for **3**, 6.963Å for **4**, 11.085 Å for **5**, and 9.836 Å for **6**, respectively. It is worth pointing out that the pbmb ligands act as pillars in **1**, leading to a 3D pillar-layered framework. In **2** and **3**, pbmb ligands connect Zn(II) or Cd(II) ions constructing a $[Zn(pbmb)]_n$ or ($[Cd(pbmb)]_n$) linear chain. In **4**, the pbmb ligands join Zn(II) ions in an elliptical ring, which may further stabilize the 2D layers. And in **5**, pbmb ligands connecting Zn(II) ions support the 1D Zn(II)/$bpdc^2$ chain to generate a 2D layer. Furthermore, the pbmb ligands link two adjacent Cd(II) ions to produce discrete dinuclear subunits in compound **6**.

Finally, the combination of carboxylate groups and pbmb ligands lead to the construction of six different topological structures: a 3D 8-connected uninodal **sqc3** topology framework for **1**, a (4,4) 2D grid layer for **2**, **3** and **5**, a 2D (3,4,5)-connected topological network for **4**, and a 1D double-chain structure for **6**. The results indicate that the different species of functional groups, as well as the number and position of the carboxylic groups in the carboxylates, have crucial influences on the final structures for compounds **1**−**6**.

Powder X-ray diffraction analyses and thermogravimetric analyses

To characterize the phase purities of compounds **1**−**6**, powder X-ray diffraction (PXRD) patterns have been checked at ambient temperature (Fig. S1). For **1**−**6**, the measured PXRD patterns agree with those calculated from the X-ray single crystal diffraction data, demonstrating the phase purity of the compounds. By contrast, the slight differences in intensities may be attributed to the preferred orientation of the crystalline powder samples.

In order to investigate the mobility of the solvent molecules within the MOFs, TGA was carried out for **1–6**, and the results are shown in Fig. 7. For anhydrous **1**, the decomposition of the organic ligands occurs from the temperature of 295 °C for **1**. The remaining weight loss is in accordance with the formation of Ag_2O (observed: 32.35% and calculated: 31.56% for **1**). The TG curves for **2**, **3**, **4** and **6** show the initial weight loss below 150 °C, which can be ascribed to the

CrystEngComm Accepted Manuscript

removal of coordinated and lattice water molecules (observed: 2.35% and calculated: 2.07% for **2**; observed: 2.12% and calculated: 1.7% for **3**; observed: 2.84% and calculated: 2.56% for **4**; observed: 3.08% and calculated: 2.80 % for **6**). Further weight loss observed above 260 °C indicates the decomposition of the coordination framework. The remaining residues are 10.86% (calculated: 9.38 %) for **2** and 23.96% (calculated: 23.15 %) for **4** corresponding to the formation of ZnO; 14.78% (calculated: 14.04 %) for **3** and 21.04% (calculated: 19.94 %) for **6** corresponding to the formation of CdO. For complex **5**, the TG curve shows the initial weight loss below 120 °C, which can be ascribed to the removal of the lattice water molecule (observed: 1.99% and calculated: 2.17%). Further weight loss observed above 320 °C indicates the decomposition of the organic ligands. The residue corresponds to the formation of ZnO (observed: 20.46% and calculated: 19.60%). The results indicate that all the title compounds exhibit good thermal stabilities.

Photoluminescence Properties

Coordination polymers with d^{10} metal centers and conjugated organic linkers are promising candidates for photoactive materials with potential applications such as chemical sensors and photochemistry [25]. Hence, the solid-state photoluminescent spectra of complexes **1**−**6**, pbmb ligand and all of the carboxylic acids were investigated at ambient temperature, as depicted in Fig. 8 and Fig.S2. The free pbmb ligand shows a relatively weak emission band at 350 nm (λ_{ex} = 310 nm). It can be presumed that this peak originate from the $\pi^* \rightarrow n$ or $\pi^* \rightarrow \pi$ transitions. The photoluminescent spectra of 2,6-H_2napdc, H_2tbta, H_4btec, H_2bpdc, $H_2$3-npa show a different emission peak at 440 nm (λ_{ex} = 410 nm), 385 nm (λ_{ex} = 250 nm), 395 nm (λ_{ex} = 285 nm), 406 nm (λ_{ex} = 300 nm) and 395 nm (λ_{ex} = 250 nm), respectively. Complexes **2**−**6** exhibit their emission maxima at 390 nm upon excitation at 245 nm, while **1** exhibits its emission maxima at 400 nm upon excitation at 290 nm. For **1** and **5**, the emission bands are blue-shifted (40 nm and 16 nm, respectively) compared with that of the free carboxylate ligands, indicating that the coordination of the 2,6-H_2napdc and H_2bpdc ligands to metal ions increases the rigidity, leading to less

CrystEngComm Accepted Manuscript

vibrations of the skeleton and reducing the loss of energy by radiationless decay of the intraligand emission excited state. The fluorescent emission observed in **2−4** and **6** may be tentatively assigned to the intraligand fluorescence since the free H_2tbta, H_4btec and $H_2$3-npa ligands exhibited a similar emission under the same condition [26]. In comparison with the free ligand pbmb, the emissions in the six complexes **1−6** are red-shifted, which could most probably be due to the decreased energy gaps between the highest occupied molecular orbital (HOMO) and the lowest unoccupied molecular orbital (LUMO) of the ligands when coordinating to the metal ions [27]. The results indicate that the co-ligands have an important effect on the photoluminescence behavior.

Catalytic activities

The diffuse-reflectance UV−vis spectra reveal the absorption features of compounds **1-6** (Fig. 9), and all spectra consist of absorption components in the UV region. The main intense absorption peaks at 262, 260, 270 and 252 nm for **2**, **3**, **4** and **6**, and compounds **1** and **5** show broad absorption bands at 273 and 316 nm, can be attributed to π−π* transitions of the ligands. Moreover, the band gap energy of the material can be calculated according to the formula: Eg=1240/λg (eV). Where Eg is band gap energy (eV) and λg is absorption edge wavelength (nm). The solid-state compounds **1-6** thus shows a semiconducting character with a band gap of 2.82, 3.54, 3.54, 3.26, 2.95, 3.76 eV, respectively. It should be noted that the charge-transfer transition of **1-6** occurs in the UV region, which may be given a higher photocatalytic activities with UV-light [28].

To study the photocatalytic behavior of complexes **1–6** in detail, methyl orange was selected as a model dye contaminant to evaluate the efficiency of catalytic degradation in purifying wastewater. The methyl orange solution was carried out by persulfate activated with the complex as catalyst. The degradation process of methyl orange without any catalyst was also studied as the control experiment. In photocatalytic process pH is an important factor, so, it is vital to know and control the pH in order to enhance the photocatalytic efficiency. Five pH values (pH=1.0, 3.0, 5.0, 7.0 and 9.0) were chosen in experiment. We found that all the complexes show the highest

CrystEngComm Accepted Manuscript

ptotocatalytic activities in the case of pH =3 (Fig. 10). The catalytic efficiency of complexes **1-6** in the different pH values are given in the support information (Fig. S3).

As show in Fig. 10, all the synthetic coordination polymers demonstrate obvious catalytic behavior to decompose the methyl orange solution, especially complexes **1** and **3-6**. The total catalytic degradation efficiency of the control experiment is 20.0% after 120 min. In comparison with one, the systems with different catalysts **1-6** indicate more higher degradation efficiency for methyl orange (**1**: 99%, **2**: 66%, **3**: 91%, **4**: 83%, **5**: 91%, **6**: 93%, respectively) after 120 min in the photo-Fenton-like process. The color of the solutions changed obviously, from red to purple or even colorless. The complexes can catalyze persulfate to produce more strongly oxidizing sulfate radicals ($SO_4^{\cdot -}$) [29] and further increase the efficiency of the pollutant degradation significantly in photo-Fenton-like process.

The results display that complexes **1**, **3**, **5** and **6** are more efficient than other complexes. Curiously, complex 1, which is a silver coordination polymer, exhibits the highest photocatalytic efficiency. HOMO–LUMO gap terminology may be utilized to describe the discrete character of the light-induced transitions in the MOFs[9k,27].

During the photocatalytic process, the stabilities of compounds **1-6** were monitored by PXRD, which demonstrated that the coordination polymers were unchanged after the photocatalytic experiments, indicating the crystal materials were stable and reproducible for the degrading methyl orange in photo-Fenton-like process (Fig. S4).

The total organic carbon concentration is very important because it is one of the best observations to conclude the exact point in time when methyl orange has been entirely degraded and the complete mineralization has been achieved. Degradation of methyl orange in presence of the solid catalysts caused about 72%, 38%, 67%, 54%, 63% and 69% reduction of TOC after 120 min in photo-Fenton-like process, respectively. While the mineralization degrees (reduction percent of TOC) reached after 120 min for the methyl orange solution without catalyst at each pH and with persulfate (see table S3) are range from 10.6% to 15.2%. Thus, the above results indicate

CrystEngComm Accepted Manuscript

that UV light activation of persulphate by compounds 1-6 caused not only rapid degradation of methyl orange, but also its significant reduction of TOC, indicating mineralization.

Conclusion

In summary, tuned by different aromatic polycarboxylates and pbmb as main ligand, six Cd(II)/Ag(I)/Zn(II) coordination polymers with different dimensionalities and structures were purposefully synthesized by the hydrothermal technique. The various dimension and structural features of the six complexes may be attributed to the different coordination modes of the carboxylate groups. Additionally, the conformations of the pbmb ligand play an important role in governing the final structures.

Supporting Information Available: X-ray crystallographic data in CIF format, table S1, table S2, table S3, PXRD patterns for 1-6, photoluminescent spectra of pure carboxylic acids and the experiment results of the photocatalytic degradation of methyl orange in different pH values (Fig.S1–S4). This material is available free of charge via the Internet at http://pubs.rsc.org.

Acknowledgments

The project was supported by the National Natural Science Foundation of China (51474086) and the Hercules Foundation (project AUGE/11/029“3D-SPACE: 3D Structural Platform Aiming for Chemical Excellence”) for funding.

References

[1] (a) J. R. Long, O. M. Yaghi, *Chem. Soc. Rev.*, 2009, **38**, 1213; (b) A. Kondo, H. Kajiro, `H. Noguchi, L. Carlucci, D. M. Proserpio, G. Ciani, K. Kato, M. Takata, H. Seki, M. Sakamoto, Y. Hattori, F. Okino, K. Maeda, T. Ohba, K. Kaneko and H. Kanoh, *J. Am. Chem.Soc.*, 2011, **133**, 10512; (c) T. R. Cook, Y. R. Zheng, P. J. Stang, *Chem. Rev.*, 2013, **113**, 734; (d) F. Sun, Z. Yin, Q. Q. Wang, D. Sun, M. H. Zeng and M. Kurmoo, *Angew. Chem., Int. Ed.,* 2013, **125**, 4636; (e) W. Xuan, C. Zhu, Y. Liu, Y. Cui, *Chem. Soc. Rev.*, 2012, **41**, 1677; (f) S. R. Batten, N. R. Champness, X. M. Chen, J. Garcia-Martinez, S. Kitagawa, L. Ohrstrom, M. O’Keeffe, M. P. Suh, J. Reedijk, *Pure Appl. Chem.*, 2013, **85**, 1715.

CrystEngComm Accepted Manuscript

[2] (b) X. H. Bu, M. L. Tong, H. C. Chang, S. Kitagawa, S. R. Batten, *Angew. Chem.*, 2004, **116**, 194; (b) L. L. Fan, D. R. Xiao, E. B. Wang, Y. G. Li, Z. M. Su, X. L. Wang, J. Liu, *Cryst. Growth Des*., 2007, **7**, 592; (c) M. I. Bodnarchuk, R. Erni, F. Krumeich, M. V. Kovalenko, *Nano Lett*., 2013, **13**, 1699. (d) Y. Liu, K. Mo, Y. Cui, *Inorg. Chem.,* 2013, **52**, 10286.

[3] (a) B. Moulton and M. J. Zaworotko, *Chem. Rev.*, 2011, **101**, 1629; (b) G. P. Zhou, Y. L. Yang, R. Q. Fan, W. Cao and B. Yang, *CrystEngComm*, 2012, **14**, 193; (c) P. Wang, R. Q. Fan, Y. L. Yang, X. R. Liu, W. W. Cao and B. Yang, *J. Solid StateChem.*, 2012, **196**, 441; (d) R. Q. Fan, L. Y. Wang, P. Wang, H. Chen, C. F. Sun, Y. L. Yang and Q. Su, *J. Solid State Chem.*, 2012, **196**, 332; (e) P. Wang, R. Q. Fan, X. R. Liu, L. Y. Wang, Y. L. Yang, W. W. Cao, B. Yang, W. Hasi, Q. Su and Y. Mu, *CrystEngComm*, 2013, **15**, 1931.

[4] (a) X. C. Huang, J. P. Zhang, Y. Y. Lin and X. M. Chen, *Chem. Commun.*, 2005, 2232; (b) Y. Q. Lan, S. L. Li, X. L. Wang, K. Z. Shao, Z. M. Su and E. B. Wang, *Inorg. Chem.*, 2008, **47**, 529; (c) X. L. Wang, C. Qin, E. B. Wang, Y. G. Li, Z. M. Su, L. Xu, L. Carlucci, *Angew. Chem., Int. Ed.*, 2005, **44**, 5824; (d)Y. F. Zhou, F. L. Jiang, D. Q. Yuan, B. L. Wu, R. H. Wang, Z. Z. Lin and M. C. Hong, *Angew. Chem., Int. Ed.*, 2004, **43**, 5665.

[5] (a) P. V. Dau, K. K. Tanabe and S. M. Cohen, Chem. Commun., 2012, **48**, 9370; (b) Q. Liu, L. N. Jin and W. Y. Sun, Chem. Commun., 2012, **48**, 8814; (c) J. Yang, J. F. Ma, S. R. Batten and Z. M. Su, Chem. Commun., 2008, 2233; (d) V. A. Blatov, M. O'Keeffe and D. M. Proserpio, CrystEngComm, 2010, **12**, 44; (e) H. Fu, C. Qin, Y. Lu, Z. M. Zhang, Y. G. Li, Z. M. Su, W. L. Li, E. B. Wang, *Angew. Chem., Int. Ed.*, 2012, **51**, 7985; (f) S. C. Chen, R. R. Qin, Z. H. Zhang, J. Qin, H. B. Gao, F. A. Sun, M. Y. He and Q. Chen, *Inorg. Chim. Acta*, 2012, **390**, 61; (g) M. Wriedt, A. A. Yakovenko, G. J. Halder, A. V. Prosvirin, K. R. Dunbar and H. C. Zhou, J. Am. Chem. Soc., 2013, 135, 4040; (h) F. F. Pan, R. Wang and U. Englert, *Inorg. Chem.*, 2012, **51**, 769; (i) J. C. Geng, C. J. Wang, F. Wang, H. R. Luo, C. C. Zhao and G. H. Cui, *Chin, J. Inorg. Chem.*, 2012, **28**, 1060.

[6] (a) M. Suh, Y. Cheon and E. Lee, *Coord. Chem. Rev.*, 2008, **252**, 1007; (b) Y. J. Cui, Y. F.

CrystEngComm Accepted Manuscript

Yue, G. D. Qian and B. L. Chen, *Chem. Rev.*, 2012, **112**, 1126; (c) B. Lebeau and P. Innocenzi, *Chem. Soc. Rev.*, 2011, **40**, 886; (d) S. T. Meek, J. A. Greathouse and M. D. Allendorf, *Adv. Mater.*, 2011, **23**, 249; (e) C. G. Silva, A. Corma and H. Garcia, *J. Mater. Chem.*, 2010, **20**, 3141.

[7] (a) Thirumurugan and S. Natarajan, *J. Mater. Chem.*, 2005, **15**, 4588; (b) D. C. Zhong, J. H. Deng, X. Z. Luo, H. J. Liu, J. L. Zhong, K. J. Wang and T. B. Lu, *Cryst. Growth Des.*, 2012, **12**, 1992; (c) L. B. Sun, Y. Li, Z. Q. Liang, J. H. Yu and R. R. Xu, *Dalton Trans.*, 2012, **41**, 12790; (d) G. Liu and H. Li, *CrystEngComm*, 2013, **15**, 6870; (e) J. J. Wang, T. T. Wang, L. Tang, X. Y. Hou, L. J. Gao, F. Fu and M. L. Zhang, *J. Coord. Chem.*, 2013, **66**, 3979.

[8] (a) S. Sanda, S. Parshamoni, A. Adhikary, S. Konar, *Cryst. Growth Des.*, 2013, **13**, 5442; (b) X. He, X. P. Lu, Z. F. Ju, C. J. Li, Q. K. Zhang, M. X. Li, *CrystEngComm*, 2013, **15**, 2731; (c) M. Li, Q. Ling, Z. Yang, B. L. Li, H. Y. Li, *CrystEngComm*, 2013, **15**, 3630; (d) X. J. Wang, T. H. Huang, L. H. Tang, Z. M. Cen, Q. L. Ni, L. C. Gui, X. F. Jiang, H. K. Liu, *CrystEngComm*, 2010, **12**, 4356.

[9] (a) C. Y. Xu, L. K. Li, Y. P. Wang, Q. Q. Guo, X. J. Wang, H. W. Hou and Y. T. Fan, *Cryst. Growth Des.*, 2011, **11**, 4667; (b) C. Y. Xu, Q. Q. Guo, X. J. Wang, H. W. Hou and Y. T. Fan, *Cryst. Growth Des.*, 2011, **11**, 1869; (c) L. Liu, Y. H. Liu, D. Q. Wu, H. W. Hou and Y. T. Fan, *Inorg. Chim. Acta*, 2012, **391**, 66; (d) L. Liu, C. Huang, Z. C. Wang, D. Q. Wu, H. W. Hou and Y. T. Fan, *CrystEngComm*, 2013, **15**, 7095; (e) Q. Q. Guo, C. Y. Xu, B. Zhao, Y. Y. Jia, H. W. Hou and Y. T. Fan, *Cryst. Growth Des.*, 2012, **12**, 5439; (f) J. M. Hao, H. Zhang, G. Y. Li and G. H. Cui, *J. Coord. Chem.*, 2014, **67**, 1992; (g) L. Qin, Y. H. Li, P. J. Ma, G. H. Cui, *J. Mol. Struc.*, 2013, **1051**, 215; (h) J. M. Hao, Y. N. Zhao, R. Yang, G. H. Cui, *J. Mol. Struc.*, 2014, **1070**, 58; (i) L. Liu, J. Ding, C. Huang, M. Li, H. W. Hou, Y. T. Fan, *Cryst. Growth Des.*, 2014, **14**, 3035; (j) X. X. Wang, B. Y. Yu, K. V. Hecke, G. H. Cui, *RSC Adv.* 2014, **4**, 61281; (k) C. C. Wang, J. R. Li, X. L. Lv, Y. Q. Zhang and G. S. Guo, *Energy Environ. Sci.*, 2014, **7**, 2831.

CrystEngComm Accepted Manuscript

[10] (a) E. Q. Gao, Z. M. Wang, C. S. Liao and C. H. Yan, *New J. Chem.*, 2002, **26**, 1096; (b) K. O. Ashiry, Y. H. Zhao, K. Z. Shao, Z. M. Su, Y. M. Fu and X. R. Hao, *Inorg. Chem. Commun.*, 2008, **11**, 1181; (c) J. Y. Hu, J. P. Li, J. A. Zhao, H. W. Hou and Y. T. Fan, *Inorg. Chim. Acta*, 2009, **362**, 5023.

[11] (a) H. Kim and M. Y. P. Suh, *Inorg. Chem.*, 2005, **44**, 810; (b) Y. Qiu, H. Deng, S. Yang, J. Mou, C. Daiguebonne,N. Kerbellec, O. Guillou and S. R. Batten, *Inorg. Chem.*, 2009, **48**, 4158.

[12] (a) Y. Peng, D. Fu, R. Liu, F. Zhang, X. Liang, *Chemosphere*, 2008, **71**, 990; (b) X. R. Xu, X. Z. Li, *Sep. Purif. Technol.*, 2010, **72**, 105.

[13] K. C. Chen, J. Y. Wu, C. C. Huang, Y. M. Liang, S. C. J. Hwang, *J. Biotechnol.*, 2003, **101**, 241.

[14] W. H. Glaze, J. W. Kang, D. H. Chapin, *Ozone Sci. Eng.*, 1987, **9**, 335.

[15] T. K. Lau, W. Chu, N. J. D. Graham, *Environ. Sci. Technol.*, 2007, **41**, 613.

[16] (a) L. Qin, J. Zheng, S. L. Xiao, X. H. Zheng, G. H. Cui, *Inorg. Chem. Commun.*, 2013, 34, 71; (b) D. Zhao, X. Y. Liao, X. l. Yan, S. G. Hulingc, T. Chaia, H. Tao, *J. Hazard. Mater.*, 2013, **2254–2255**, 228.

[17] R. Bronisz, *Inorg. Chem.*, 2005, **44**, 4463; (b) C. B. Aakeröy, J. Desper, B. Leonard and J. F. Urbina, *Cryst. Growth Des.*, 2005, **5**, 865.

[18] G. M. Sheldrick, SADABS, Program for area detector adsorption correction, Institute for Inorganic Chemistry, University of Go ¨ ttingen, Germany, 1996.

[19] G. M. Sheldrick, *Acta Crystallogr. A*, 2008, **64**, 112.

[20] A. L.Spek, *Acta Cryst.* 2009, **D65**, 148.

[21] M. Qin, H. Yang, S. Chen, H. Xie, J. Guan, *Quimica Nova*, 2012, **35**, 559.

[22] L. Yang, D. R. Powell, R. P. Houser, *Dalton Trans*, 2007, **9**, 955.

[23] V. A. Blatov, *Struct Chem*, 2012, **23**, 955.

[24] M. Li, L. Liu, L. Zhang, X. F. Lv, J. Ding, H. W. Hou, Y. T. Fan, *CrystEngComm*, 2014, **16**,

CrystEngComm Accepted Manuscript

6408.

[25] (a) Q. Wu, M. Esteghamatian, N. X. Hu, Z. Popovic, G. Enright, Y. Tao, M. D'Iorio, S. Wang, *Chem. Mater.*, 2000, **12**, 79; (b) J. E. McGarrah, Y. J. Kim, M. Hissler, R. Eisenberg, *Inorg. Chem.*, 2001, **40**, 4510; (c) G. D. Santis, L. Fabbrizzi, M. Licchelli, A. Poggi, A. Taglietti, *Angew. Chem., Int. Ed.*, 1996, **35**, 202; (d) H. Y. Bai, J. F. Ma, J. Yang, Y. Y. Liu, H. Wu, J. C. Ma, *Cryst. Growth Des.*, 2010, **10**, 995.

[26] (a) V. J. Catalano and A. L. Moore, *Inorg. Chem.*, 2005, **44**, 6558; (b) B. Liu, W. Chen and S. Jin, *Organometallics*, 2007, **26**, 3660; (c) F. J. B. dit Dominique, H. Gornitzka, A. Sournia-Saquet and C. Hemmert, *Dalton Trans.*, 2009, 340.

[27] R.Y. Huang, G. X. Liu, H. M. Xu, S. Nishihara, X. M. Ren, *J Chem Crystallogr*, 2012, **42**, 416.

[28] (a) L Liu, J Ding, C Huang, M Li, H. W. Hou, Y. T. Fan, *Cryst. Growth Des.,* 2014, **14**, 3035; (b) L. L. Wen, J.B. Zhao, K.L. Lv, Y. H. Wu, K. J. Deng, X. K. Leng, D. F. Li, *Cryst. Growth Des.,* 2012, **12**, 1603.

[29] M.C. Yeber, L. Díaz, J. Fernández, J. Photochem. *Photobiol. A: Chem.*, 2010, **215**, 90.

CrystEngComm Accepted Manuscript

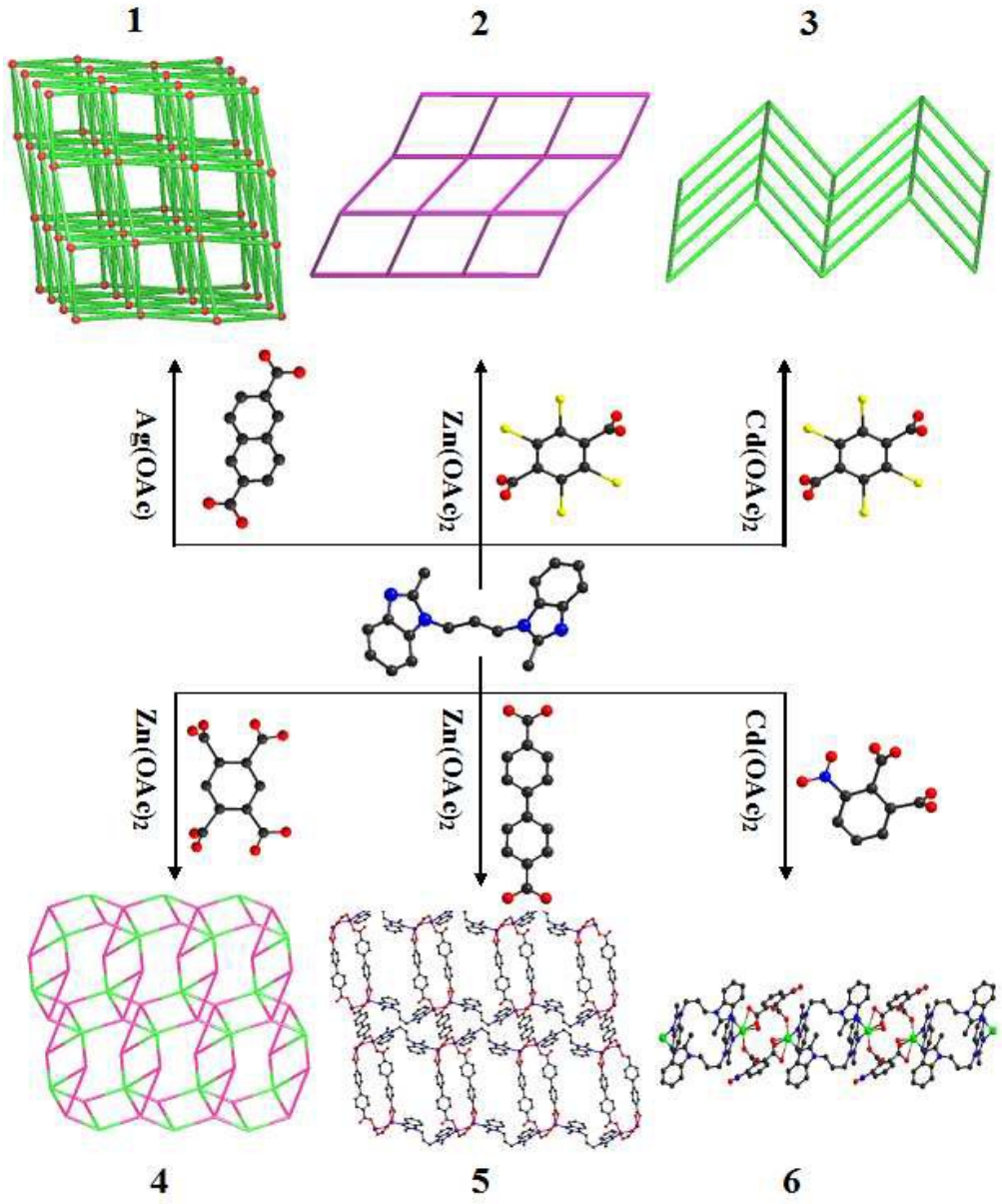

Scheme 1 Synthetic strategies and structure diversity for compounds **1**−**6**

CrystEngComm Accepted Manuscript

Fig. 1 (a) Coordination environment around the Ag(I) centers in complex **1**. Hydrogen atoms are omitted for clarity. (Symmetry code: A: -*x*+1/2,*y*+1/2,-*z*+3/2; B: *x*-1/2,-*y*+5/2,*z*-1/2; C: -*x*,-*y*+2,-*z*+2; D: -*x*+1/2,*y*-1/2,-*z*+5/2) **(b)** Polyhedral representation of the coordination geometry of the Ag^{+} centre. **(c)** Intricate coordination modes of 2,6-napdc^{2-} anions. **(d)** Tetranuclear Ag(I)-cluster $[Ag_4(COO)_4]^{8+}$ as secondary building unit (SBU) in complex **1**. (**e**) 2D (4,4) layer constructed by Ag(I)-clusters. **(f)** View of the 3D coordination framework of **1**. **(g)** Schematic representation of the 8-connected uninodal **sqc3** topology with a point symbol of $\{4^2 4.6^4\}$.

Fig. 2 (a) Coordination environment around the Zn(II) centers in complex **2**. Hydrogen atoms are omitted for clarity. (Symmetry code: A: -*x*+1/2,*y*,-*z*+1/2) **(b)** Polyhedral representation of the coordination geometry of the Zn^{2+} centre. **(c)** Perspective view of the 2D layer in **2**. **(d)** Simplified view of the 2D supramolecular net reinforced via O–H···O hydrogen bonding interactions. **(e)** View of the 3D supramolecular framework formed through weak π–π interactions.

Fig. 3 (a) Coordination environment around the Cd(II) centers in complex **3**. Hydrogen atoms are omitted for clarity. (Symmetry code: A: *x*,*y*-1,*z*; B: -*x*+1,-*y*,-*z*+2) **(b)** Polyhedral representation of the coordination geometry of the Cd^{2+} centre. **(c)** Perspective view of the 2D layer in **3**. **(d)** View of the 3D supramolecular framework formed through weak π–π interactions.

Fig. 4 (a) Coordination environment around the Zn(II) centers in complex **4**. Hydrogen atoms are omitted for clarity. (Symmetry code: A: -*x*+2,-*y*+2,-*z*-1; B: -*x*+2,-*y*+2,-*z*; C: *x*+1,*y*,*z*) **(b)** Polyhedral representation of the coordination geometry of the Zn^{2+} centre. **(c)** Intricate coordination modes of btec^{4-} anions. **(d)** View of the 2D layer generated by btec^{4-}. **(e)** Simplified view of the (3,4,5)-connected 2D network in **4**. **(f)** View of the 3D supramolecular architecture via weak π−π interactions in **4.**

Fig. 5 (a) Coordination environment around the Zn(II) centers in complex **5**. Hydrogen atoms are omitted for clarity. (Symmetry code: A: -*x*+1,-*y*+1,-*z*+2; B: *x*+1,*y*,*z*; C: -*x*+1,-*y*,-*z*+1) **(b)** Polyhedral representation of the coordination geometry of the Zn^{2+} centre. **(c)** Intricate coordination modes of the bpdc^{2-} anions. **(d)** View of the 1D loop-like chain generated by bpdc^{2-}

CrystEngComm Accepted Manuscript

anions. **(e)** View of the 2D coordination layer in **5**. **(f)** Simplified view of the 3D 2-fold interpenetrating (3,6)-connected supramolecular net in **5.**

Fig. 6 (a) Coordination environment around the Cd(II) centers in the complex **6**. Hydrogen atoms are omitted for clarity. (Symmetry code: A: -*x*,-*y*+1,-*z*+2; B: -*x*,-*y*,-*z*+1) **(b)** Polyhedral representation of the coordination geometry of the Cd^{2+} centre. **(c)** View of the 1D double-chain structure in **6**. **(d)** View of the 3D supramolecular architecture via hydrogen bonding interactions in **6. (e)** Simplified view of the 3D (4,5,5)-connected supramolecular net in **6**.

Fig. 7 TGA curves for complexes **1**-**6**.

Fig. 8 Solid-state photoluminescent spectra of free pbmb and complexes **1**-**6**.

Fig. 9 UV−vis diffuse-reflectance spectra of compounds **1** to **6** with $BaSO_4$ as background.

Fig. 10 The experiment results of the photocatalytic degradation of methyl orange (pH=3).

CrystEngComm Accepted Manuscript

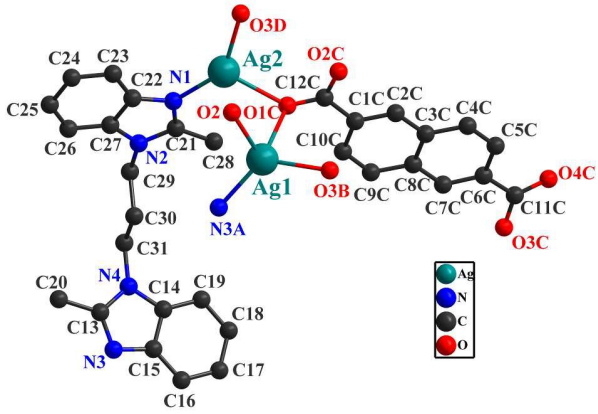

(a)

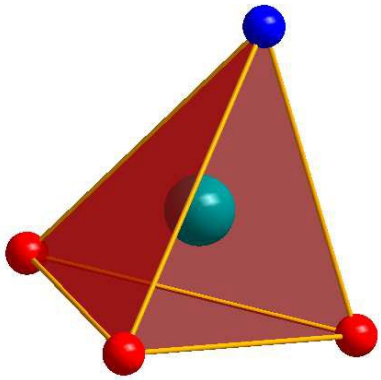

(b)

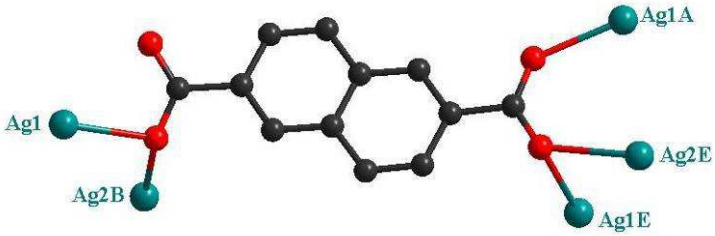

(c)

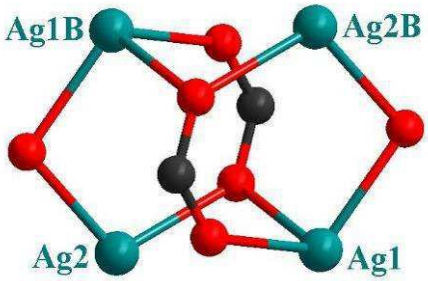

CrystEngComm Accepted Manuscript

(d)

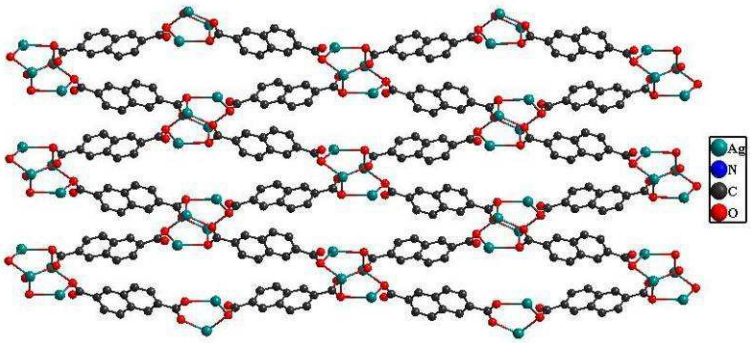

(e)

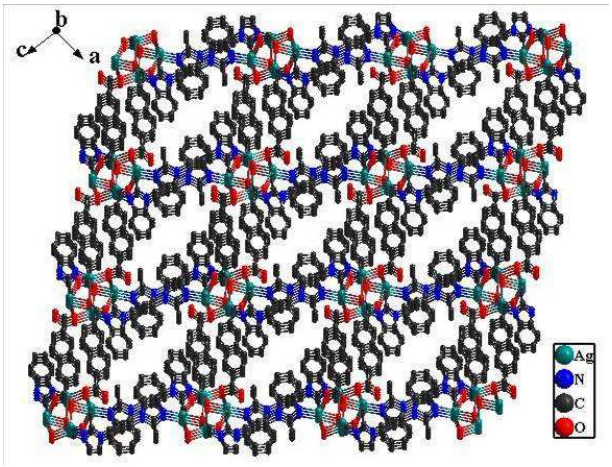

(f)

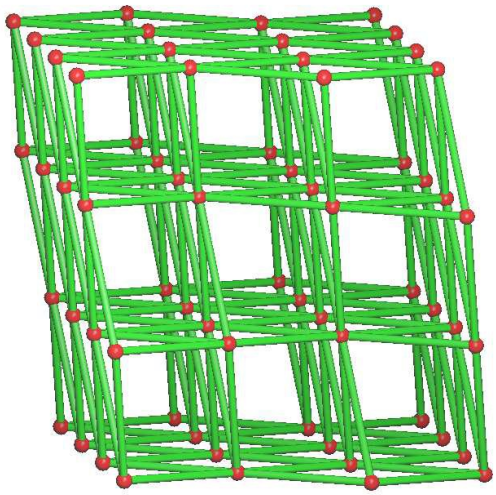

(g)

CrystEngComm Accepted Manuscript

Fig. 1 (a) Coordination environment around the Ag(I) centers in complex **1**. Hydrogen atoms are omitted for clarity. (Symmetry code: A: -*x*+1/2,*y*+1/2,-*z*+3/2; B: *x*-1/2,-*y*+5/2,*z*-1/2; C: -*x*,-*y*+2,-*z*+2; D: -*x*+1/2,*y*-1/2,-*z*+5/2) **(b)** Polyhedral representation of the coordination geometry of the Ag^{+} centre. **(c)** Intricate coordination modes of 2,6-napdc^{2-} anions. **(d)** Tetranuclear Ag(I)-cluster $[Ag_4(COO)_4]^{8+}$ as secondary building unit (SBU) in complex **1**. (**e**) 2D (4,4) layer constructed by Ag(I)-clusters. **(f)** View of the 3D coordination framework of **1**. **(g)** Schematic representation of the 8-connected uninodal **sqc3** topology with a point symbol of $\{4^2 4.6^4\}$.

CrystEngComm Accepted Manuscript

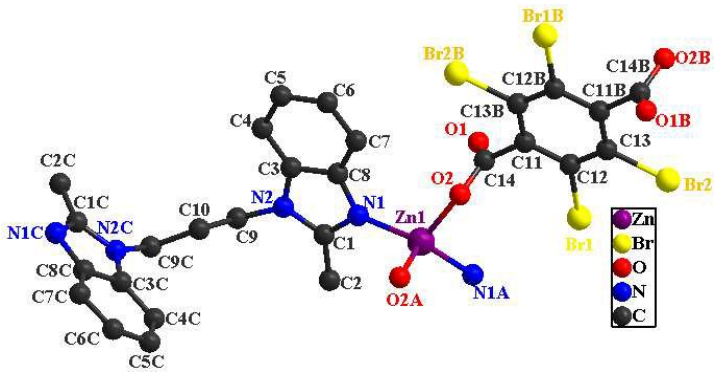

(a)

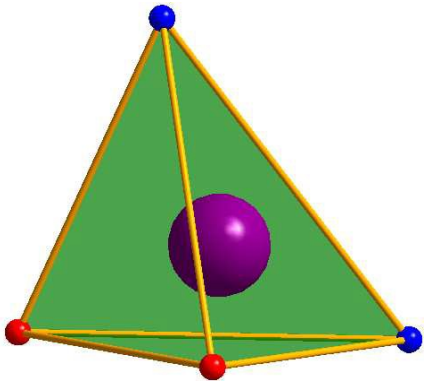

(b)

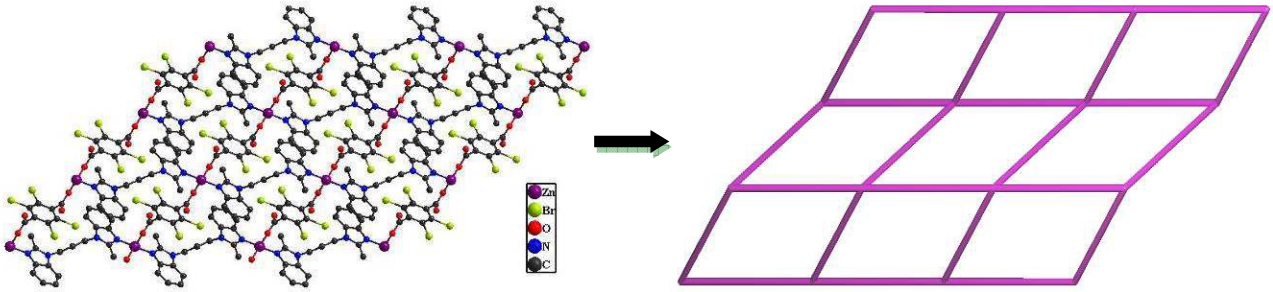

(c)

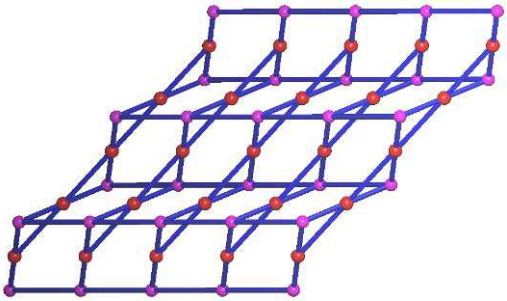

CrystEngComm Accepted Manuscript

(d)

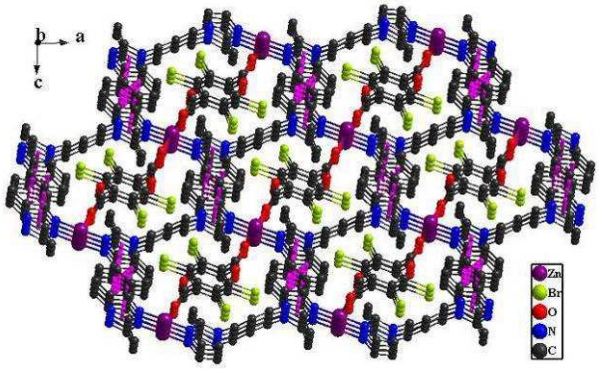

(e)

Fig. 2 (a) Coordination environment around the Zn(II) centers in complex **2**. Hydrogen atoms are omitted for clarity. (Symmetry code: A: -*x*+1/2,*y*,-*z*+1/2) **(b)** Polyhedral representation of the coordination geometry of the Zn^{2+} centre. **(c)** Perspective view of the 2D layer in **2**. **(d)** Simplified view of the 2D supramolecular net reinforced via O–H···O hydrogen bonding interactions. **(e)** View of the 3D supramolecular framework formed through weak π–π interactions.

CrystEngComm Accepted Manuscript

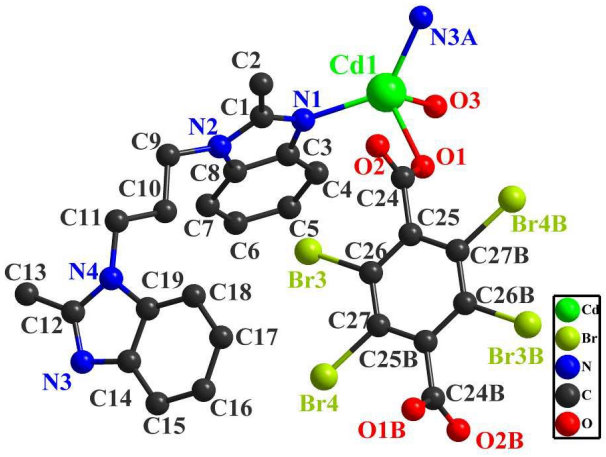

(a)

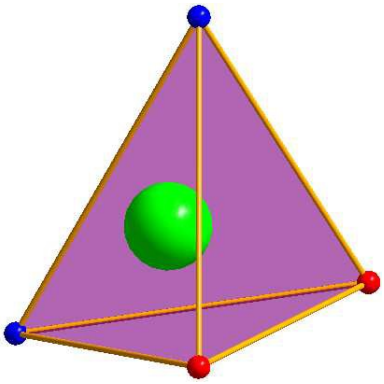

(b)

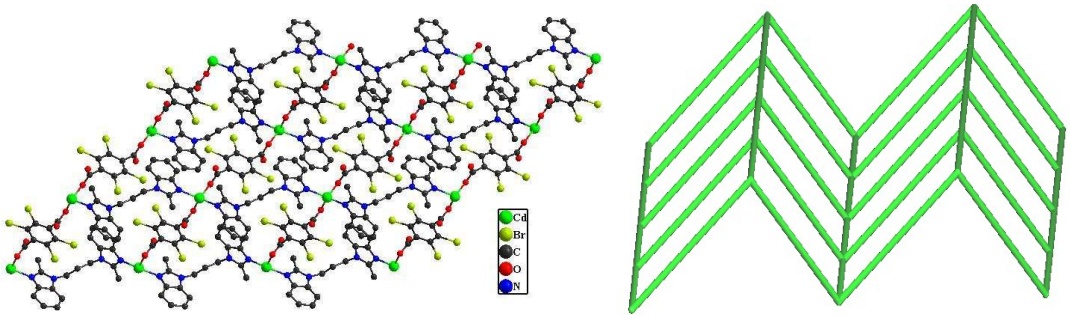

(c)

CrystEngComm Accepted Manuscript

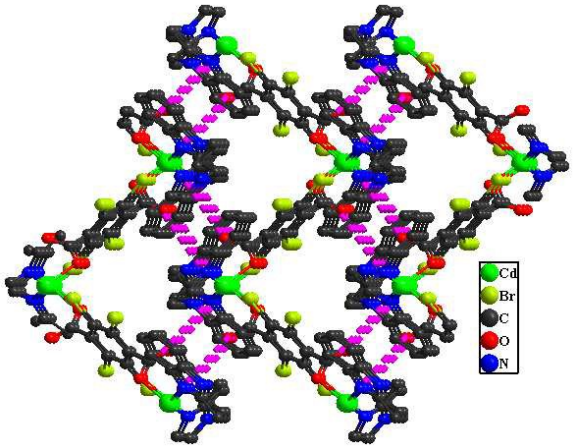

(d)

Fig. 3 (a) Coordination environment around the Cd(II) centers in complex **3**. Hydrogen atoms are omitted for clarity. (Symmetry code: A: *x*,*y*-1,*z*; B: -*x*+1,-*y*,-*z*+2) **(b)** Polyhedral representation of the coordination geometry of the Cd^{2+} centre. **(c)** Perspective view of the 2D layer in **3**. **(d)** View of the 3D supramolecular framework formed through weak π–π interactions.

CrystEngComm Accepted Manuscript

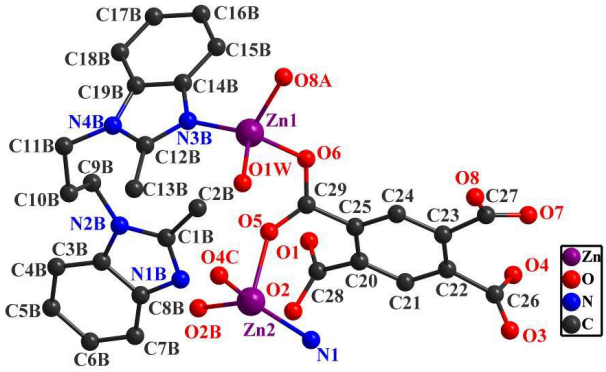

(a)

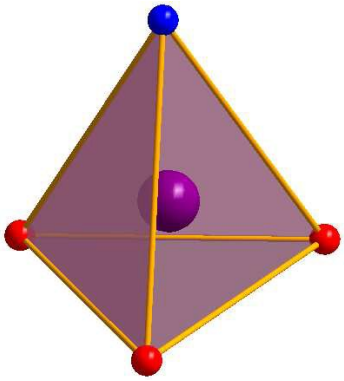

(b)

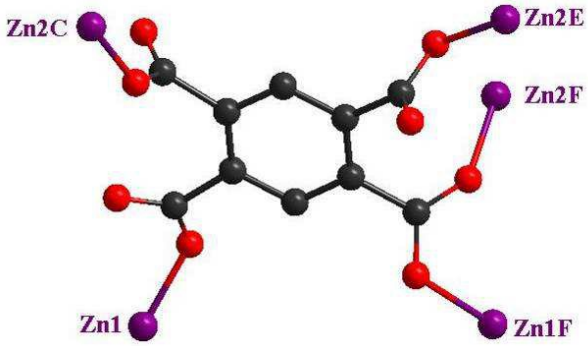

(c)

CrystEngComm Accepted Manuscript

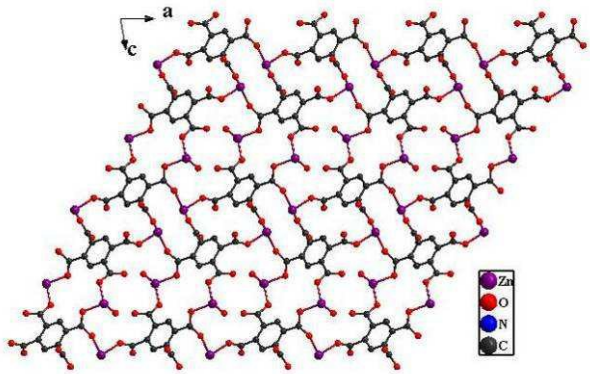

(d)

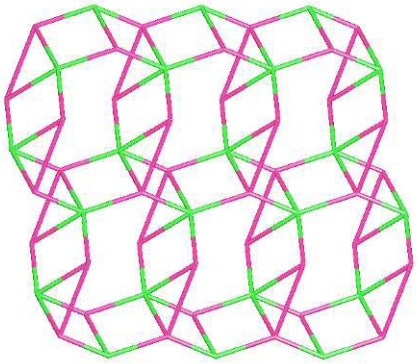

(e)

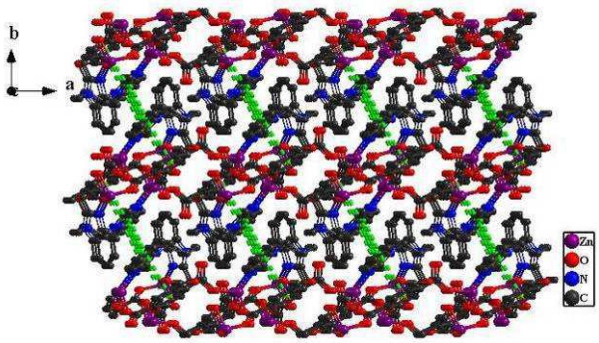

(f)

Fig. 4 (a) Coordination environment around the Zn(II) centers in complex **4**. Hydrogen atoms are omitted for clarity. (Symmetry code: A: -*x*+2,-*y*+2,-*z*-1; B: -*x*+2,-*y*+2,-*z*; C: *x*+1,*y*,*z*) **(b)** Polyhedral representation of the coordination geometry of the Zn^{2+} centre. **(c)** Intricate coordination modes of $btec^{4-}$ anions. **(d)** View of the 2D layer generated by $btec^{4-}$. **(e)** Simplified

CrystEngComm Accepted Manuscript

view of the (3,4,5)-connected 2D network in **4**. **(f)** View of the 3D supramolecular architecture via weak $\pi-\pi$ interactions in **4.**

CrystEngComm Accepted Manuscript

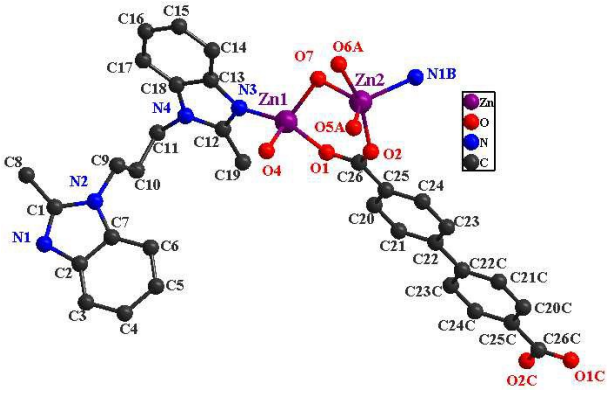

(a)

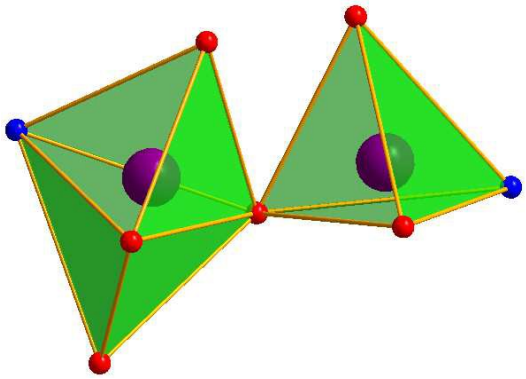

(b)

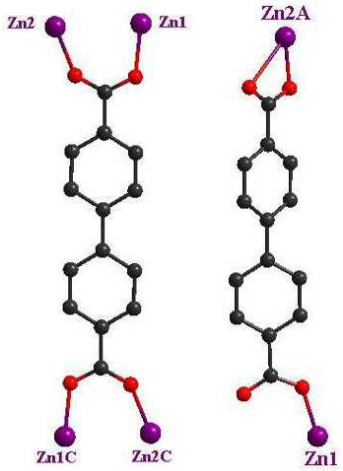

(c)

CrystEngComm Accepted Manuscript

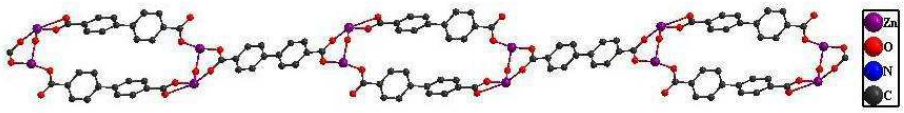

(d)

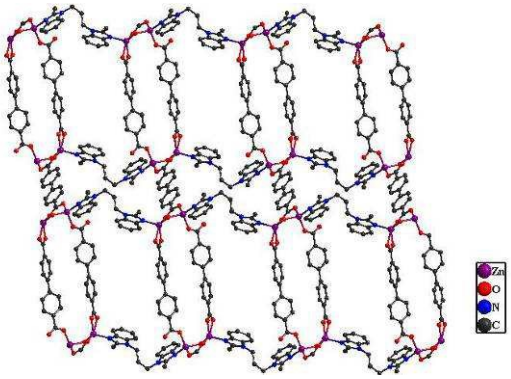

(e)

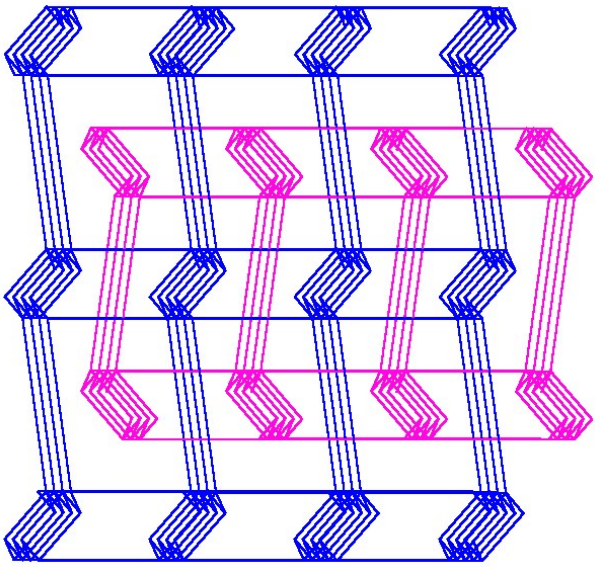

(f)

Fig. 5 (a) Coordination environment around the Zn(II) centers in complex **5**. Hydrogen atoms are omitted for clarity. (Symmetry code: A: -*x*+1,-*y*+1,-*z*+2; B: *x*+1,*y*,*z*; C: -*x*+1,-*y*,-*z*+1) **(b)** Polyhedral representation of the coordination geometry of the Zn^{2+} centre. **(c)** Intricate coordination modes of the $bpdc^{2-}$ anions. **(d)** View of the 1D loop-like chain generated by $bpdc^{2-}$

CrystEngComm Accepted Manuscript

anions. **(e)** View of the 2D coordination layer in **5**. **(f)** Simplified view of the 3D 2-fold interpenetrating (3,6)-connected supramolecular net in **5.**

CrystEngComm Accepted Manuscript

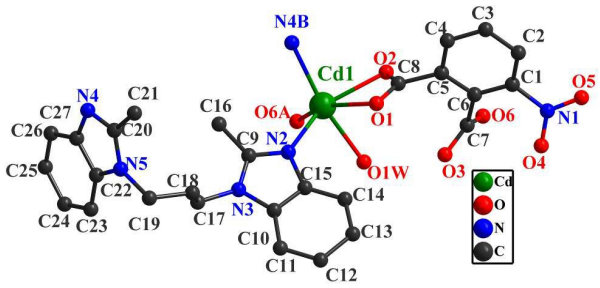

(a)

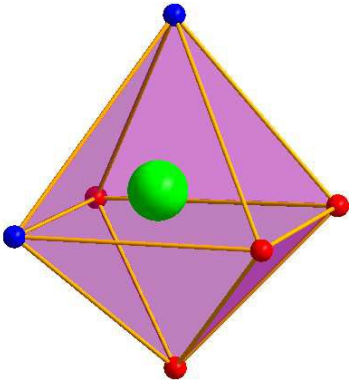

(b)

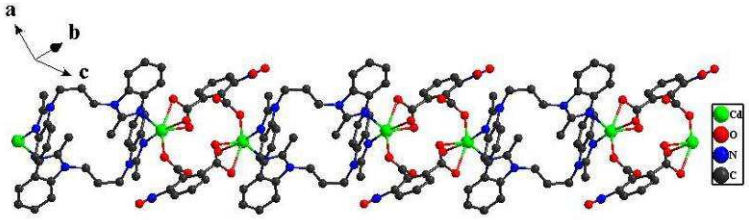

(c)

CrystEngComm Accepted Manuscript

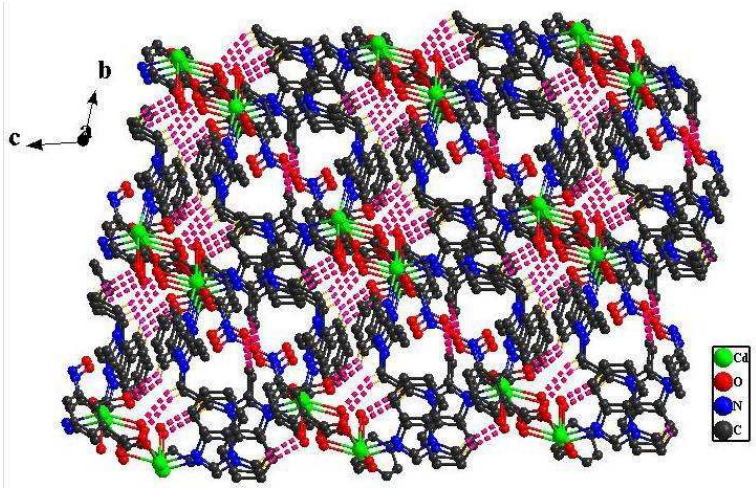

(d)

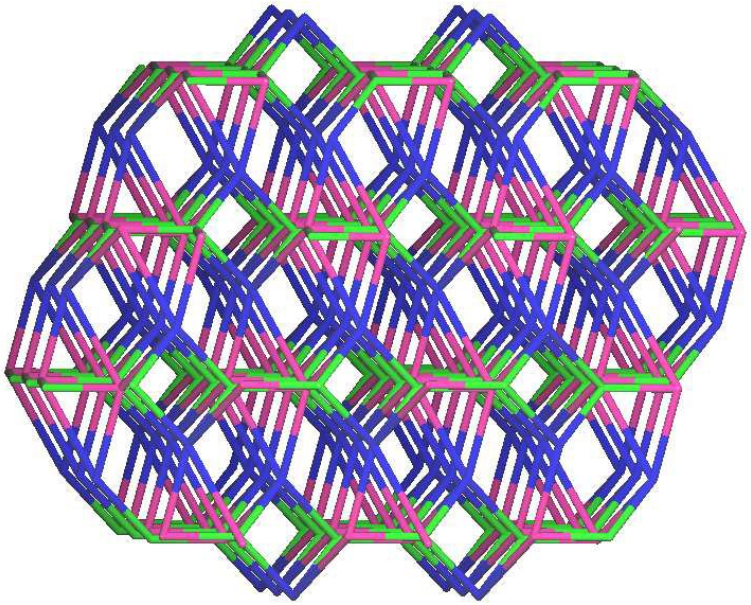

(e)

Fig. 6 (a) Coordination environment around the Cd(II) centers in the complex **6**. Hydrogen atoms are omitted for clarity. (Symmetry code: A: -*x*,-*y*+1,-*z*+2; B: -*x*,-*y*,-*z*+1) **(b)** Polyhedral representation of the coordination geometry of the Cd^{2+} centre. **(c)** View of the 1D double-chain structure in **6**. **(d)** View of the 3D supramolecular architecture via hydrogen bonding interactions in **6. (e)** Simplified view of the 3D (4,5,5)-connected supramolecular net in **6**.

CrystEngComm Accepted Manuscript

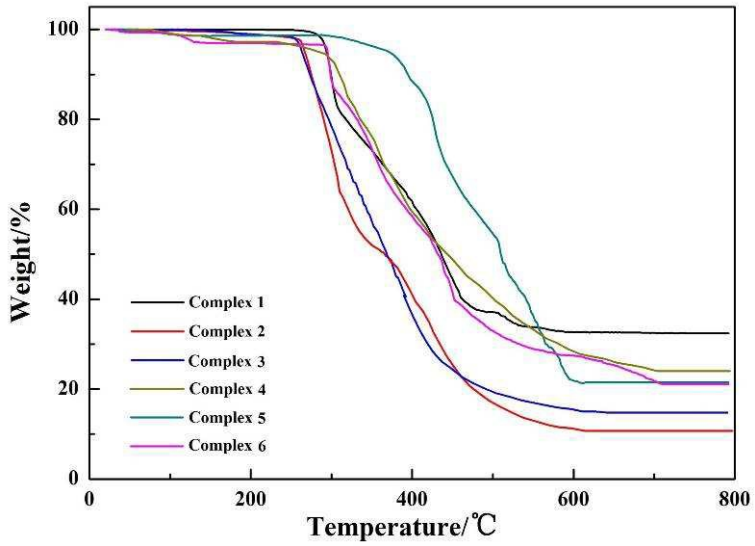

Fig. 7 TGA curves for complexes **1**-**6**.

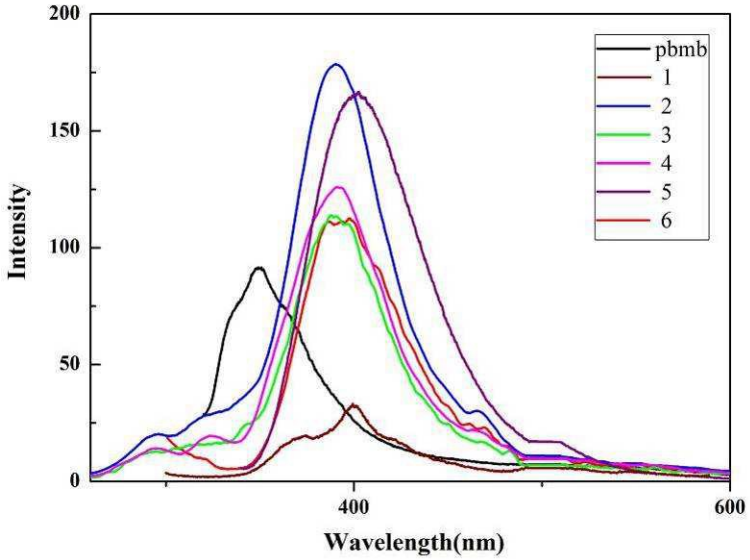

Fig. 8 Solid-state photoluminescent spectra of free pbmb and complexes **1**-**6**.

CrystEngComm Accepted Manuscript

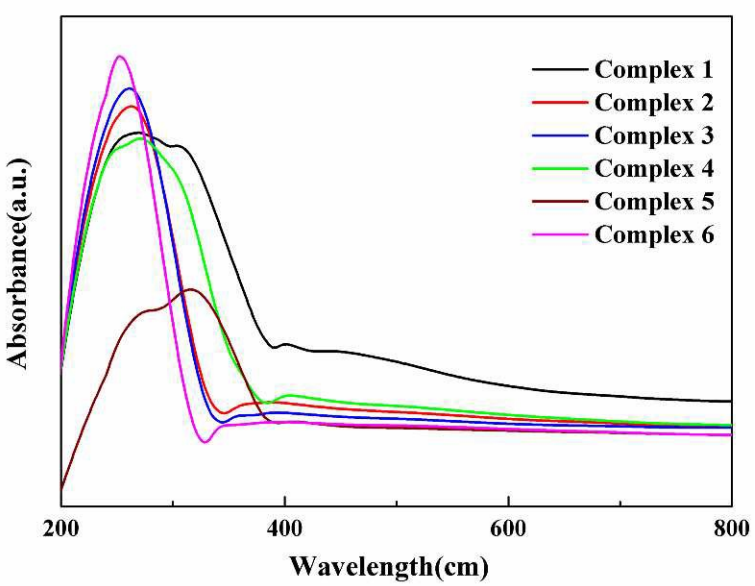

Fig. 9 UV−vis diffuse-reflectance spectra of compounds **1** to **6** with $BaSO_4$ as background.

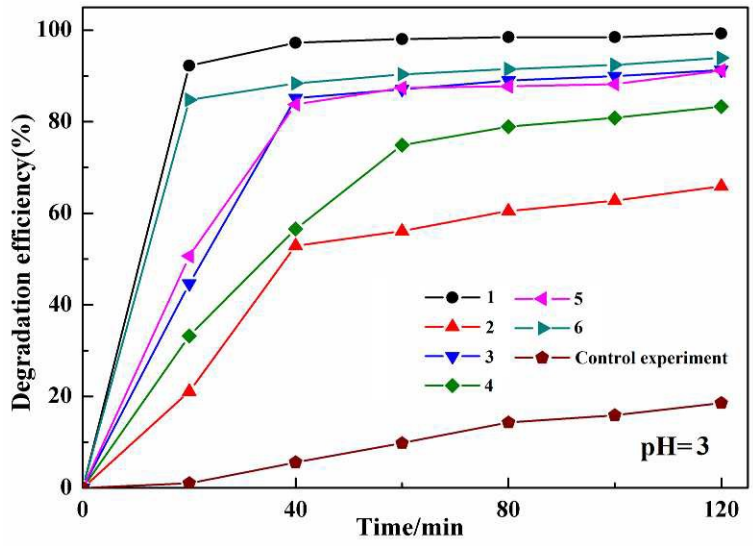

Fig. 10 The experiment results of the photocatalytic degradation of methyl orange (pH=3).

CrystEngComm Accepted Manuscript

Graphical Abstract

Six d^{10} metal coordination polymers have been prepared by a hydrothermal technique employing a flexible ligand 1,1'-(1,3-propane)bis-(2-methylbenzimidazole) (pbmb) with d^{10} metal ions in the presence of various carboxylate coligands. Complex **1**-**6** possess structural diversities from 1D to 3D and interesting topologies. Moreover, all of the materials manifest high catalytic activities for the degradation of methyl orange in the photo-Fenton process.

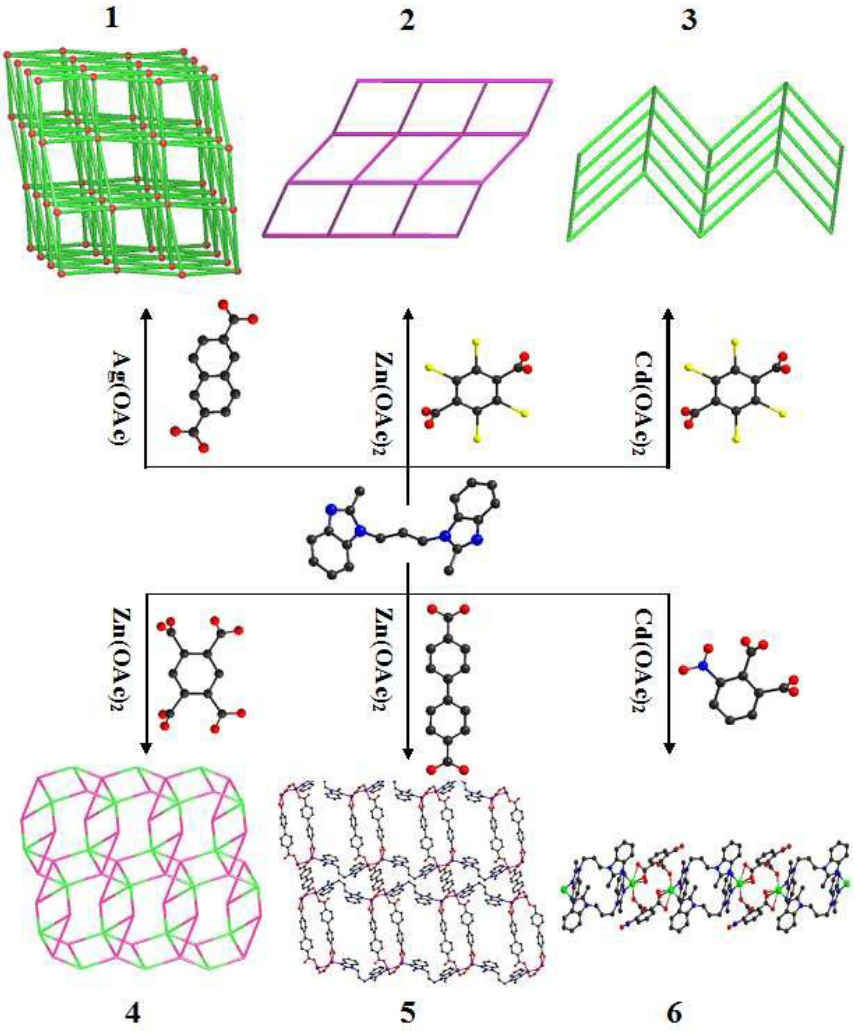

CrystEngComm Accepted Manuscript